A CLD-Coreset Selection Algorithm

For completeness, we provide the full pseudocode for the coreset selection procedure described in Section 4.1. This algorithm computes per-class CLD scores by correlating each training sample's loss trajectory with the corresponding class-specific validation trajectory, and selects a fixed number of top-scoring samples per class to form a class-balanced coreset.

Algorithm 1: Coreset Selection Using CLD (Per-Class)

Input: Training set $\mathbf{S} = \{\vec{z}_m\}_{m=1}^{N}$, Validation set $\mathbf{V} = \{\vec{q}_j\}_{j=1}^{Q}$, Class budgets $\{k_c\}_{c=1}^{C}$ with $k = \sum_{c=1}^{C} k_c$, Epochs T, Initial params $\theta_{\mathbf{S}}^0$, Loss ℓ, Optimizer $\mathcal{A}$, Hyperparameters λ

Output: Coreset $\mathbf{C}$ of size k

for $t \leftarrow 1$ **to** T **do**
  $\theta_{\mathbf{S}}^t \leftarrow \mathcal{A}(\theta_{\mathbf{S}}^{t-1}, \mathbf{S}, \lambda)$ `// update model`
  for $m \leftarrow 1$ **to** N **do**
    Store $\ell(\theta_{\mathbf{S}}^t, \vec{z}_m)$ `// record train loss`
  for $j \leftarrow 1$ **to** Q **do**
    Store $\ell(\theta_{\mathbf{S}}^t, \vec{q}_j)$ `// record val loss`
for $m \leftarrow 1$ **to** N **do**
  $\vec{\Delta}(\vec{z}_m) \leftarrow \left[\ell(\theta_{\mathbf{S}}^t, \vec{z}_m) - \ell(\theta_{\mathbf{S}}^{t-1}, \vec{z}_m)\right]_{t=1}^{T}$
for $j \leftarrow 1$ **to** Q **do**
  $\vec{\Delta}(\vec{q}_j) \leftarrow \left[\ell(\theta_{\mathbf{S}}^t, \vec{q}_j) - \ell(\theta_{\mathbf{S}}^{t-1}, \vec{q}_j)\right]_{t=1}^{T}$
for $c \leftarrow 1$ **to** C **do**
  $\mathbf{S}_c \leftarrow \{\vec{z}_m \in \mathbf{S} : y_m = c\}$;
  $\mathbf{V}_c \leftarrow \{\vec{q}_j \in \mathbf{V} : y_j = c\}$;
  $\vec{\Delta}'_{\mathbf{V},c} \leftarrow \frac{1}{|\mathbf{V}_c|} \sum_{\vec{q}_j \in \mathbf{V}_c} \vec{\Delta}(\vec{q}_j)$;
  foreach $\vec{z}_m \in \mathbf{S}_c$ **do**
    $\texttt{CLD}(\vec{z}_m) \leftarrow \rho\big(\vec{\Delta}(\vec{z}_m),\, \vec{\Delta}'_{\mathbf{V},c}\big)$
  $\mathbf{C}_c \leftarrow$ top-k_c elements of $\mathbf{S}_c$ by $\texttt{CLD}(\vec{z}_m)$;
$\mathbf{C} \leftarrow \bigcup_{c=1}^{C} \mathbf{C}_c$;
return $\mathbf{C}$

B Detailed Theoretical Framework

In this appendix, we provide the complete theoretical framework supporting the results stated in Section 5. We first outline the detailed lemmas establishing gradient alignment and approximation properties of CLD-selected coresets. We then conclude with a full proof of the convergence guarantee presented in Theorem 1.

B.1 Supporting Lemmas for Theorem 1

Lemma 1 (High CLD Implies Gradient Alignment)**.** *Consider a training sample $\vec{z}_m \in \mathbf{S}$ with $\texttt{CLD}(\vec{z}_m) = \rho\big(\vec{\Delta}(\vec{z}_m), \vec{\Delta}'_{\mathbf{V}}\big) \geq 1 - \epsilon$ for some small $\epsilon > 0$. Let $\theta_{\mathbf{S}}^t$ be the parameters obtained by running algorithm $\mathcal{A}$ on $\mathbf{S}$ for t iterations. Let $\delta\theta^{t-1} := \theta_{\mathbf{S}}^t - \theta_{\mathbf{S}}^{t-1}$ be the parameter update at step t.*

Suppose the learning algorithm is run for a sufficiently large number of iterations T. Assume the sequence of parameter updates $\{\delta\theta^{t-1}\}_{t=1}^{T}$ is sufficiently varied. This means the updates are not persistently orthogonal to any fixed non-zero vector direction in the relevant parameter subspace.

Then, for most training steps t where $G_{\mathbf{V}}(\theta_{\mathbf{S}}^t) \neq 0$, the sample gradient $\nabla_\theta \ell(\theta_{\mathbf{S}}^t, \vec{z}_m)$ and the validation gradient $G_{\mathbf{V}}(\theta_{\mathbf{S}}^t)$ are well-aligned:

$$\cos\left(\angle\left(\nabla_\theta \ell(\theta_{\mathbf{S}}^t, \vec{z}_m), G_{\mathbf{V}}(\theta_{\mathbf{S}}^t)\right)\right) \geq 1 - \epsilon'_t, \tag{17}$$

where $\epsilon'_t \to 0$ *as* $\epsilon \to 0$.

Proof. We first analyze the idealized case where the correlation is perfect ($\epsilon = 0$) and the underlying approximations hold exactly, and then argue by continuity.

Assume the first-order Taylor expansions are exact for the loss changes:

$$\big(\vec{\Delta}(\vec{z}_m)\big)_t = \ell(\theta_{\mathbf{S}}^t, \vec{z}_m) - \ell(\theta_{\mathbf{S}}^{t-1}, \vec{z}_m) \approx \langle \nabla_\theta \ell(\theta_{\mathbf{S}}^{t-1}, \vec{z}_m), \delta\theta^{t-1} \rangle = x_t, \tag{18}$$

$$(\vec{\Delta}'_{\mathbf{V}})_t = \frac{1}{Q} \sum_{j=1}^{Q} \big(\ell(\theta_{\mathbf{S}}^t, \vec{q}_j) - \ell(\theta_{\mathbf{S}}^{t-1}, \vec{q}_j)\big) \approx \langle G_{\mathbf{V}}(\theta_{\mathbf{S}}^{t-1}), \delta\theta^{t-1} \rangle = y_t. \tag{19}$$

Assume perfect correlation $\rho(\vec{x}, \vec{y}) = 1$.
This implies an exact positive linear relationship $x_t = c\, y_t + K'$ for all t, where $c = \sigma_x / \sigma_y > 0$ and $K' = \overline{x} - c\,\overline{y}$.
Substituting the definitions of x_t and y_t:

$$\langle \nabla_\theta \ell(\theta_{\mathbf{S}}^{t-1}, \vec{z}_m), \delta\theta^{t-1} \rangle = c\, \langle G_{\mathbf{V}}(\theta_{\mathbf{S}}^{t-1}), \delta\theta^{t-1} \rangle + K'. \tag{20}$$

Rearranging yields:

$$\langle \nabla_\theta \ell(\theta_{\mathbf{S}}^{t-1}, \vec{z}_m) - c\, G_{\mathbf{V}}(\theta_{\mathbf{S}}^{t-1}), \delta\theta^{t-1} \rangle = K'. \tag{21}$$

Since the mean of the loss trajectory will be smaller compared to the variance of the terms (losses eventually reduce to 0), it is reasonable to assume $K' \approx 0$.
Thus, for $t = 1, \ldots, T$:

$$\langle \nabla_\theta \ell(\theta_{\mathbf{S}}^{t-1}, \vec{z}_m) - c\, G_{\mathbf{V}}(\theta_{\mathbf{S}}^{t-1}), \delta\theta^{t-1} \rangle = 0. \tag{22}$$

Let $\vec{w}_{t-1} \coloneqq \nabla_\theta \ell(\theta_{\mathbf{S}}^{t-1}, \vec{z}_m) - c\, G_{\mathbf{V}}(\theta_{\mathbf{S}}^{t-1})$.
The vector $\vec{w}_{t-1}$ is exactly orthogonal to the update direction $\delta\theta^{t-1}$ at each step t.

Now, invoke the assumption that the sequence of updates $\{\delta\theta^{t-1}\}_{t=1}^T$ is sufficiently varied.
This means the updates are not persistently orthogonal to any fixed non-zero direction $\vec{w}_{t-1}$.
If $\vec{w}_{t-1}$ were non-zero, the variation in updates would eventually yield a $\delta\theta^{t-1}$ such that $\langle \vec{w}_{t-1}, \delta\theta^{t-1} \rangle \neq 0$.
Since the inner product is exactly zero for all t in our idealized case, the only possibility consistent with the sufficient variation assumption is that $\vec{w}_{t-1}$ must be the zero vector. Thus:

$$\vec{w}_{t-1} = \nabla_\theta \ell(\theta_{\mathbf{S}}^{t-1}, \vec{z}_m) - c\, G_{\mathbf{V}}(\theta_{\mathbf{S}}^{t-1}) = \vec{0}. \tag{23}$$

This signifies that the sample gradient is exactly a positive scalar multiple ($c > 0$) of the validation gradient:

$$\nabla_\theta \ell(\theta_{\mathbf{S}}^{t-1}, \vec{z}_m) = c\, G_{\mathbf{V}}(\theta_{\mathbf{S}}^{t-1}). \tag{24}$$

Consequently, the vectors are perfectly collinear and point in the same direction (assuming $G_{\mathbf{V}}(\theta_{\mathbf{S}}^{t-1}) \neq 0$).
The angle γ_{t-1} between them is exactly 0. Therefore, in this idealized case:

$$\cos(\gamma_{t-1}) = \cos\big(\angle\big(\nabla_\theta \ell(\theta_{\mathbf{S}}^{t-1}, \vec{z}_m), G_{\mathbf{V}}(\theta_{\mathbf{S}}^{t-1})\big)\big) = 1. \tag{25}$$

This derivation holds under the ideal conditions ($\epsilon = 0$, exact Taylor approx., $K' = 0$).
Since the involved operations are continuous, when the conditions are only approximately met (i.e., $\rho \geq 1 - \epsilon$ with $\epsilon \to 0$, Taylor approx. is good, K' is small), the resulting cosine similarity will be close to 1.
We express this conclusion as

$$\cos(\gamma_{t-1}) \geq 1 - \epsilon'_{t-1}, \tag{26}$$

where the error $\epsilon'_{t-1} \to 0$ as $\epsilon \to 0$.
Assuming this alignment holds for most steps t (implying alignment at step t relies on properties at $t-1$), the lemma statement follows. □

Remark 2 (On Update Sequence Variation)**.** *The assumption regarding the update sequence* $\{\delta\theta^{t-1}\}$ *is that it exhibits enough variation over the trajectory to ensure that no fixed non-zero vector can remain orthogonal to all updates. This property is weaker than requiring the updates to span the entire parameter space, but it is sufficient for the argument. It essentially prevents the gradient difference vector from hiding in a direction that the optimization process never explores. Stochastic optimization methods accumulating updates over many iterations (large* T*) are often expected to satisfy this sufficient variation condition.*

Lemma 2 (Stability of Gradient Alignment)**.** *Suppose the conditions in Theorem 1 hold: specifically, L-smoothness and bounded gradients ($\|\nabla_\theta \ell(\theta, \vec{z})\|_2 \le B$ for all $\vec{z}$). Consider a coreset $\mathbf{C}$ constructed by selecting samples with high* CLD *scores:*

$$\mathbf{C} = \{\vec{z}_m \in \mathbf{S} : \texttt{CLD}(\vec{z}_m) \ge 1 - \epsilon\}, \quad \textit{with} \quad |\mathbf{C}| = k \ , \ \epsilon > 0, \ \epsilon \to 0. \tag{27}$$

Assume that during training, the difference between the parameter trajectories satisfies $\|\theta^t_{\mathbf{C}} - \theta^t_{\mathbf{S}}\|_2 = \|\delta_t\|_2$ at step t.

Then, for each sample $\vec{z}_m \in \mathbf{C}$, the cosine similarity between its gradient and the average validation gradient at step t is lower bounded by

$$\cos\left(\angle\left(\nabla_\theta \ell(\theta^t_{\mathbf{C}}, \vec{z}_m), G_{\mathbf{V}}(\theta^t_{\mathbf{C}})\right)\right) \ge 1 - \kappa, \tag{28}$$

where $\kappa = \epsilon'_t + \frac{4L}{B}\|\delta_t\|_2 + \frac{3L^2}{B^2}\|\delta_t\|_2^2$, and $\epsilon'_t \to 0$ as $\epsilon \to 0$.

Proof. Let $\omega_m = \nabla_\theta \ell(\theta^t_{\mathbf{C}}, \vec{z}_m) - \nabla_\theta \ell(\theta^t_{\mathbf{S}}, \vec{z}_m)$ and $\omega_{\mathbf{V}} = G_{\mathbf{V}}(\theta^t_{\mathbf{C}}) - G_{\mathbf{V}}(\theta^t_{\mathbf{S}})$ denote the deviations between gradients evaluated on the coreset trajectory and the full dataset trajectory.

By L-smoothness of $\ell(\cdot, \vec{z}_m)$ and of the validation-average loss $\hat{R}_{\mathbf{V}}(\theta) \coloneqq \frac{1}{Q}\sum_{j=1}^{Q} \ell(\theta, \vec{q}_j)$, we have:

$$\|\omega_m\|_2 \le L\|\delta_t\|_2, \tag{29}$$
$$\|\omega_{\mathbf{V}}\|_2 \le L\|\delta_t\|_2. \tag{30}$$

Expanding the inner product:

$$\langle \nabla_\theta \ell(\theta^t_{\mathbf{C}}, \vec{z}_m), G_{\mathbf{V}}(\theta^t_{\mathbf{C}})\rangle = \langle \nabla_\theta \ell(\theta^t_{\mathbf{S}}, \vec{z}_m) + \omega_m, G_{\mathbf{V}}(\theta^t_{\mathbf{S}}) + \omega_{\mathbf{V}}\rangle \tag{31}$$
$$= \langle \nabla_\theta \ell(\theta^t_{\mathbf{S}}, \vec{z}_m), G_{\mathbf{V}}(\theta^t_{\mathbf{S}})\rangle + \langle \omega_m, G_{\mathbf{V}}(\theta^t_{\mathbf{S}})\rangle + \langle \nabla_\theta \ell(\theta^t_{\mathbf{S}}, \vec{z}_m), \omega_{\mathbf{V}}\rangle + \langle \omega_m, \omega_{\mathbf{V}}\rangle. \tag{32}$$

Applying Cauchy–Schwarz inequality and the bounded gradient norm $\|\nabla_\theta \ell(\theta, \vec{z})\|_2 \le B$, we have:

$$\langle \omega_m, G_{\mathbf{V}}(\theta^t_{\mathbf{S}})\rangle \ge -\|\omega_m\|_2 \left\|G_{\mathbf{V}}(\theta^t_{\mathbf{S}})\right\|_2 \ge -LB\|\delta_t\|_2, \tag{33}$$
$$\langle \nabla_\theta \ell(\theta^t_{\mathbf{S}}, \vec{z}_m), \omega_{\mathbf{V}}\rangle \ge -\left\|\nabla_\theta \ell(\theta^t_{\mathbf{S}}, \vec{z}_m)\right\|_2 \|\omega_{\mathbf{V}}\|_2 \ge -LB\|\delta_t\|_2, \tag{34}$$
$$\langle \omega_m, \omega_{\mathbf{V}}\rangle \ge -\|\omega_m\|_2 \|\omega_{\mathbf{V}}\|_2 \ge -L^2\|\delta_t\|_2^2. \tag{35}$$

Thus,

$$\langle \nabla_\theta \ell(\theta^t_{\mathbf{C}}, \vec{z}_m), G_{\mathbf{V}}(\theta^t_{\mathbf{C}})\rangle \ge \langle \nabla_\theta \ell(\theta^t_{\mathbf{S}}, \vec{z}_m), G_{\mathbf{V}}(\theta^t_{\mathbf{S}})\rangle - 2LB\|\delta_t\|_2 - L^2\|\delta_t\|_2^2. \tag{36}$$

The denominator is upper bounded by:

$$\left\|\nabla_\theta \ell(\theta^t_{\mathbf{C}}, \vec{z}_m)\right\|_2 \left\|G_{\mathbf{V}}(\theta^t_{\mathbf{C}})\right\|_2 \le (B + L\|\delta_t\|_2)^2. \tag{37}$$

Combining this result with Lemma 1, we can conclude:

$$\cos\left(\angle\left(\nabla_\theta \ell(\theta^t_{\mathbf{C}}, \vec{z}_m), G_{\mathbf{V}}(\theta^t_{\mathbf{C}})\right)\right) \ge 1 - \left(\epsilon'_t + \frac{4L}{B}\|\delta_t\|_2 + \frac{3L^2}{B^2}\|\delta_t\|_2^2\right) = 1 - \kappa, \tag{38}$$

where ϵ'_t captures the initial alignment error when training on $\mathbf{S}$. This completes the proof. □

Remark 3. *Lemma 2 shows that if a sample's gradient is well-aligned with the validation gradient during training on the full dataset (i.e., ϵ'_t is small), then this alignment is preserved when training on a coreset $\mathbf{C}$, as long as the parameter trajectories $\theta^t_{\mathbf{S}}$ and $\theta^t_{\mathbf{C}}$ remain close. The degradation in alignment is bounded by terms that are linear and quadratic in $\|\delta_t\|_2$. Thus, as long as the coreset trajectory stays near the full dataset trajectory, the generalization-relevant properties captured by* CLD *remain stable. This stability is crucial for ensuring that* CLD*-based coresets maintain the training dynamics of the full dataset.*

Remark 4 (Influence of Coreset Size on κ)**.** *It is important to explicitly consider how the coreset size $k = |\mathbf{C}|$ (as specified in Lemma 2) influences the components of $\kappa = \epsilon'_t + \frac{4L}{B} \|\delta_t\|_2 + \frac{3L^2}{B^2} \|\delta_t\|_2^2$.*

- *The term ϵ'_t, representing the initial alignment error derived from Lemma 1, is affected by k. A smaller coreset size k allows for a more stringent selection criterion for samples based on their* `CLD` *scores. Specifically, one can choose only samples with* $\texttt{CLD}(\vec{z}_m)$ *very close to* 1*, which corresponds to a smaller ϵ in the selection rule* $\texttt{CLD}(\vec{z}_m) \geq 1 - \epsilon$ *(from Theorem 1 and Lemma 2). A smaller ϵ naturally leads to a smaller ϵ'_t.*
- *Conversely, the terms in κ that depend on $\|\delta_t\|_2 = \|\theta^t_{\mathbf{C}} - \theta^t_{\mathbf{S}}\|_2$ (the deviation between coreset and full-data parameter trajectories) are also influenced by k. While a smaller k allows for higher individual sample quality, a very small k might result in a coreset that is less representative of the full dataset $\mathbf{S}$. This reduced representativeness can lead to a larger divergence $\|\delta_t\|_2$ during training, as the optimization trajectory on the small coreset may differ more substantially from that on the full data. An increase in $\|\delta_t\|_2$ would, in turn, increase the overall value of κ.*

Therefore, the selection of an appropriate coreset size k involves an inherent trade-off. A smaller k can be beneficial for the ϵ'_t component of κ by enabling the selection of higher-quality samples. However, if k is too small, it could adversely affect the components of κ related to $\|\delta_t\|_2$ by making the coreset insufficiently representative. The stability discussed in Remark 3 relies on $\|\delta_t\|_2$ remaining small, highlighting the importance of k being chosen to adequately approximate the full dataset's training dynamics while leveraging the benefits of high `CLD` *scores.*

Lemma 3 (Subset-Gradient Approximation)**.** *Suppose the conditions in Theorem 1 hold, including L-smoothness, bounded gradients, and validation representativeness as described in Section 5.*

Define the average coreset gradient at step t as

$$\gamma^t_{\mathbf{C}} = \frac{1}{|\mathbf{C}|} \sum_{m \in \mathbf{C}} \nabla_\theta \ell(\theta^t_{\mathbf{C}}, \vec{z}_m). \tag{39}$$

Then, for every training step t, we have

$$\left\|\gamma^t_{\mathbf{C}} - \nabla_\theta R_{\mathbf{D}}(\theta^t_{\mathbf{C}})\right\|_2 \leq B\sqrt{2\kappa} + \delta, \tag{40}$$

where κ captures the alignment error and satisfies $\kappa \to 0$ as $\epsilon \to 0$.

Proof. We decompose the error using the triangle inequality:

$$\left\|\gamma^t_{\mathbf{C}} - \nabla_\theta R_{\mathbf{D}}(\theta^t_{\mathbf{C}})\right\|_2 \leq \left\|\gamma^t_{\mathbf{C}} - G_{\mathbf{V}}(\theta^t_{\mathbf{C}})\right\|_2 + \left\|G_{\mathbf{V}}(\theta^t_{\mathbf{C}}) - \nabla_\theta R_{\mathbf{D}}(\theta^t_{\mathbf{C}})\right\|_2. \tag{41}$$

The second term $\|G_{\mathbf{V}}(\theta^t_{\mathbf{C}}) - \nabla_\theta R_{\mathbf{D}}(\theta^t_{\mathbf{C}})\|_2$ is bounded by δ by the validation representativeness assumption. To bound the first term $\|\gamma^t_{\mathbf{C}} - G_{\mathbf{V}}(\theta^t_{\mathbf{C}})\|_2$, we apply Jensen's inequality:

$$\left\|\gamma^t_{\mathbf{C}} - G_{\mathbf{V}}(\theta^t_{\mathbf{C}})\right\|_2^2 = \left\| \frac{1}{|\mathbf{C}|} \sum_{m \in \mathbf{C}} \left(\nabla_\theta \ell(\theta^t_{\mathbf{C}}, \vec{z}_m) - G_{\mathbf{V}}(\theta^t_{\mathbf{C}})\right) \right\|^2 \tag{42}$$

$$\leq \frac{1}{|\mathbf{C}|} \sum_{m \in \mathbf{C}} \left\|\nabla_\theta \ell(\theta^t_{\mathbf{C}}, \vec{z}_m) - G_{\mathbf{V}}(\theta^t_{\mathbf{C}})\right\|_2^2. \tag{43}$$

Define φ^t_m as the angle between $\nabla_\theta \ell(\theta^t_{\mathbf{C}}, \vec{z}_m)$ and $G_{\mathbf{V}}(\theta^t_{\mathbf{C}})$. By Lemma 2, we have $\cos\varphi^t_m \geq 1 - \kappa$ for all m. Expanding the squared distance:

$$\left\|\nabla_\theta \ell(\theta^t_{\mathbf{C}}, \vec{z}_m) - G_{\mathbf{V}}(\theta^t_{\mathbf{C}})\right\|_2^2 = \left\|\nabla_\theta \ell(\theta^t_{\mathbf{C}}, \vec{z}_m)\right\|_2^2 + \left\|G_{\mathbf{V}}(\theta^t_{\mathbf{C}})\right\|_2^2 - 2\langle \nabla_\theta \ell(\theta^t_{\mathbf{C}}, \vec{z}_m), G_{\mathbf{V}}(\theta^t_{\mathbf{C}})\rangle \tag{44}$$

$$= \left\|\nabla_\theta \ell(\theta^t_{\mathbf{C}}, \vec{z}_m)\right\|_2{}^2 + \left\|G_{\mathbf{V}}(\theta^t_{\mathbf{C}})\right\|_2^2 - 2\left\|\nabla_\theta \ell(\theta^t_{\mathbf{C}}, \vec{z}_m)\right\|_2 \left\|G_{\mathbf{V}}(\theta^t_{\mathbf{C}})\right\|_2 \cos\varphi^t_m. \tag{45}$$

Since $\|\nabla_\theta \ell(\theta^t_{\mathbf{C}}, \vec{z}_m)\|_2, \|G_{\mathbf{V}}(\theta^t_{\mathbf{C}})\|_2 \le B$ and $\cos\varphi^t_m \ge 1-\kappa$, we have

$$\left\|\nabla_\theta \ell(\theta^t_{\mathbf{C}}, \vec{z}_m) - G_{\mathbf{V}}(\theta^t_{\mathbf{C}})\right\|_2^2 \le 2B^2\kappa. \tag{46}$$

Substituting back into the Jensen bound,

$$\left\|\gamma^t_{\mathbf{C}} - G_{\mathbf{V}}(\theta^t_{\mathbf{C}})\right\|_2^2 \le 2B^2\kappa. \tag{47}$$

Taking square roots gives

$$\left\|\gamma^t_{\mathbf{C}} - G_{\mathbf{V}}(\theta^t_{\mathbf{C}})\right\|_2 \le B\sqrt{2\kappa}. \tag{48}$$

Thus, combining the two bounds,

$$\left\|\gamma^t_{\mathbf{C}} - \nabla_\theta R_{\mathbf{D}}(\theta^t_{\mathbf{C}})\right\|_2 \le B\sqrt{2\kappa} + \delta, \tag{49}$$

as claimed. □

Remark 5. *Lemma 3 shows that under mild conditions, the average gradient computed over a coreset selected based on* CLD *remains close to the true risk gradient throughout training. The deviation is controlled by two sources: the alignment error κ arising from the selection of high-*CLD *samples, and the validation approximation error δ due to finite sample size. Consequently, optimization over* CLD*-coresets closely tracks the gradient flow of the full dataset, ensuring that convergence and generalization properties are preserved. This result is crucial for connecting loss trajectory dynamics with practical coreset construction.*

B.2 Proof for Theorem 1

Proof. Define

$$R_t \coloneqq R_{\mathbf{D}}(\theta^t_{\mathbf{C}}), \qquad G_t \coloneqq \nabla_\theta R_{\mathbf{D}}(\theta^t_{\mathbf{C}}), \qquad \gamma^t_{\mathbf{C}} \coloneqq \frac{1}{|\mathbf{C}|}\sum_{m\in\mathbf{C}} \nabla_\theta \ell(\theta^t_{\mathbf{C}}, \vec{z}_m). \tag{50}$$

By L-smoothness of $\ell(\cdot)$, and in extension $R_{\mathbf{D}}(\cdot)$, and $\eta \le 1/L$,

$$R_{t+1} \le R_t + \langle G_t, \theta^{t+1}_{\mathbf{C}} - \theta^t_{\mathbf{C}}\rangle + \frac{L}{2}\left\|\theta^{t+1}_{\mathbf{C}} - \theta^t_{\mathbf{C}}\right\|_2^2. \tag{51}$$

Substituting the model update $\theta^{t+1}_{\mathbf{C}} - \theta^t_{\mathbf{C}} = -\eta\gamma^t_{\mathbf{C}}$:

$$R_{t+1} \le R_t - \eta\langle G_t, \gamma^t_{\mathbf{C}}\rangle + \frac{L\eta^2}{2}\left\|\gamma^t_{\mathbf{C}}\right\|_2^2. \tag{52}$$

Rearranging,

$$\eta\langle G_t, \gamma^t_{\mathbf{C}}\rangle \le R_t - R_{t+1} + \frac{L\eta^2}{2}\left\|\gamma^t_{\mathbf{C}}\right\|_2^2. \tag{53}$$

Decomposing the inner product using the true gradient G_t we get,

$$\langle G_t, \gamma^t_{\mathbf{C}}\rangle = \langle G_t,\, G_t + (\gamma^t_{\mathbf{C}} - G_t)\rangle = \|G_t\|_2^2 + \langle G_t, \gamma^t_{\mathbf{C}} - G_t\rangle. \tag{54}$$

Substituting this back,

$$\eta\|G_t\|_2^2 \le R_t - R_{t+1} - \eta\langle G_t, \gamma^t_{\mathbf{C}} - G_t\rangle + \frac{L\eta^2}{2}\left\|\gamma^t_{\mathbf{C}}\right\|_2^2. \tag{55}$$

Let $E_t = \|\gamma^t_{\mathbf{C}} - G_t\|_2$.
Lemma 3 under the stated assumptions gives the bound $E_t \le B\sqrt{2\kappa} + \delta$.
By Cauchy–Schwarz inequality,

$$-\eta\langle G_t, \gamma^t_{\mathbf{C}} - G_t\rangle \;\le\; \eta\|G_t\|_2\left\|\gamma^t_{\mathbf{C}} - G_t\right\|_2 = \eta\|G_t\|_2 E_t. \tag{56}$$

Young's inequality states that $ab \leq a^2/(2\gamma) + \gamma b^2/2, \quad \forall a, b \geq 0$ and $\gamma > 0$.
By using this inequality with $\gamma = 1$,

$$-\eta\langle G_t, \gamma_{\mathbf{C}}^t - G_t\rangle \;\leq\; \frac{\eta}{2}\left\|G_t\right\|_2^2 + \frac{\eta}{2}E_t^2. \tag{57}$$

Substituting this into the inequality in Equation (55),

$$\eta\left\|G_t\right\|_2^2 \leq R_t - R_{t+1} + \tfrac{\eta}{2}\left\|G_t\right\|_2^2 + \tfrac{\eta}{2}E_t^2 + \frac{L\eta^2}{2}\left\|\gamma_{\mathbf{C}}^t\right\|_2^2. \tag{58}$$

Since all gradients are bounded by B, their average $\left\|\gamma_{\mathbf{C}}^t\right\|_2$ is also bounded by B.

$$\therefore \frac{\eta}{2}\left\|G_t\right\|_2^2 \;\leq\; R_t - R_{t+1} + \frac{\eta}{2}E_t^2 + \frac{L\eta^2}{2}B^2. \tag{59}$$

Summing from $t = 0$ to $T - 1$:

$$\frac{\eta}{2}\sum_{t=0}^{T-1}\left\|G_t\right\|_2^2 \;\leq\; (R_0 - R_T) + \sum_{t=0}^{T-1}\left(\frac{\eta}{2}E_t^2 + \frac{L\eta^2}{2}B^2\right). \tag{60}$$

Let $R_{\inf} = \inf_\theta R_{\mathbf{D}}(\theta)$. Then $R_0 - R_T \leq R_0 - R_{\inf}$. Substituting the bound $E_t \leq B\sqrt{2\kappa} + \delta$:

$$\frac{\eta}{2}\sum_{t=0}^{T-1}\left\|G_t\right\|_2^2 \;\leq\; R_{\mathbf{D}}(\theta_{\mathbf{C}}^0) - R_{\inf} + T\frac{\eta}{2}(B\sqrt{2\kappa} + \delta)^2 + T\frac{L\eta^2}{2}B^2. \tag{61}$$

The sum on the left is lower bounded by T times the minimum term, i.e., $\sum_{t=0}^{T-1}\left\|G_t\right\|_2^2 \geq T \cdot \min_{0\leq t<T}\left\|G_t\right\|_2^2$.

$$\therefore \frac{\eta T}{2}\min_{0\leq t<T}\left\|G_t\right\|_2^2 \;\leq\; R_{\mathbf{D}}(\theta_{\mathbf{C}}^0) - R_{\inf} + T\frac{\eta}{2}(B\sqrt{2\kappa} + \delta)^2 + T\frac{L\eta^2}{2}B^2. \tag{62}$$

Since $\eta, T > 0$,

$$\min_{0\leq t<T}\left\|G_t\right\|_2^2 \leq \frac{2\left[R_{\mathbf{D}}(\theta_C^0) - R_{\inf}\right]}{\eta T} + (B\sqrt{2\kappa} + \delta)^2 + L\eta B^2. \tag{63}$$

This proves the theorem. □

C Datasets, Models, and Experimental Details

We evaluate our method on two standard image classification benchmarks: CIFAR-100 (Krizhevsky et al., 2009) and ImageNet-1k (Russakovsky et al., 2015). CIFAR-100 consists of 50,000 training and 10,000 test images across 100 classes and is publicly available without licensing restrictions. For ImageNet-1k, we use the official release from `https://image-net.org/download.php`, which is provided under a standard academic research license and requires user agreement to the terms of access.

Architectures. Our experiments employ the following CNN backbones:

- **ResNet-18, ResNet-34, and ResNet-50** He et al. (2016) from `https://pytorch.org/vision/stable/models/resnet.html` (BSD-3-Clause license).
- **VGG-19 with batch normalization** Simonyan & Zisserman (2014) from `https://pytorch.org/vision/stable/models/vgg.html` (BSD-3-Clause license).
- **DenseNet-121** Huang et al. (2017) from `https://pytorch.org/vision/stable/models/densenet.html` (BSD-3-Clause license).

For baseline comparisons, we use the `DeepCore` library Guo et al. (2022) (`https://github.com/PatrickZH/DeepCore`), which provides standardized implementations of several coreset selection techniques and is licensed under MIT. All training and evaluation code was implemented in PyTorch; dependencies including torchvision are MIT/BSD licensed.

Training Setup for CIFAR-100. All networks were trained using SGD Bottou (2010) for 164 epochs with an initial learning rate of 0.1, decayed by a factor of 0.1 at epochs 81 and 121. Nesterov momentum Sutskever et al. (2013) with momentum 0.9 was used, along with weight decay 5×10^{-4}. Standard augmentations included resizing to 32×32, random cropping with padding $= 4$, random horizontal flips, and normalization.

Training Setup for ImageNet-1k. Training followed standard ImageNet protocols: all models were trained with SGD for 90 epochs, with a learning rate of 0.1 decayed by 0.1 at epochs 30 and 60. Nesterov momentum with coefficient 0.9 and weight decay 10^{-4} were used. Data augmentations included random resized cropping to 224×224, horizontal flipping, and normalization.

Reproducibility. No fine-tuning or additional regularization was applied to any method, including ours, ensuring fairness in coreset comparisons. All methods used the same validation split as the validation proxy, and the same train split as the full training set available for each seed when scoring training samples. Each experiment was repeated across 5 independent runs with distinct seeds; reported results reflect the mean and standard deviation.

All experiments were conducted on a private compute cluster with access to NVIDIA A40 GPUs (48 GB memory, 300W TDP). All training and evaluation runs were performed in full precision using PyTorch.

Results. Performance results for CIFAR-100 and ImageNet-1k coreset experiments are shown in Tables 2, 3, 4, and 5. Cross-architecture transferability results for `CLD` coresets, as discussed in Section 6, are shown in Table 6.

Table 2: Performance (top-1 accuracy) of score-based coreset methods on CIFAR100 trainsplit. The coresets were selected and finetuned on ResNet-18. The full trainset performance was $\mathbf{70.95 \pm 0.68}$. The mean accuracy over 5 runs, along with their standard deviation, is reported.

Coreset Sizes	Random	Herding	Forgetting	Cal	EL2N	Moderate	CCS(AUM)	$\mathbb{D}^2$-Pruning	**CLD (Ours)**
0.2%	3.66 ± 0.41	2.57 ± 0.52	3.52 ± 0.16	5.24 ± 0.41	3.9 ± 0.45	3.8 ± 0.47	4.1 ± 0.5	4.6 ± 0.52	**5.67 ± 0.36**
0.4%	6.03 ± 0.28	3.42 ± 0.49	5.12 ± 0.53	7.46 ± 0.28	6.2 ± 0.41	6 ± 0.44	6.9 ± 0.42	7.4 ± 0.46	**7.51 ± 0.59**
0.6%	6.8 ± 0.27	4.07 ± 0.41	6.8 ± 0.18	9.12 ± 0.27	8.7 ± 0.4	8.4 ± 0.42	8.2 ± 0.38	8.6 ± 0.43	**8.91 ± 0.41**
0.8%	7.96 ± 0.79	5.14 ± 0.7	8.42 ± 0.38	10.19 ± 0.79	9.8 ± 0.48	10.2 ± 0.49	10.5 ± 0.55	10.5 ± 0.5	**10.56 ± 0.24**
1%	9.38 ± 0.41	5.32 ± 0.33	11.53 ± 0.44	13.73 ± 0.41	13.2 ± 0.46	12.7 ± 0.45	12.1 ± 0.49	13.1 ± 0.47	**13.04 ± 0.54**
2%	12.74 ± 0.28	8.29 ± 0.45	15.9 ± 0.21	16.45 ± 0.28	17 ± 0.43	16.3 ± 0.43	16.4 ± 0.46	17.5 ± 0.45	**17.05 ± 0.22**
3%	16.58 ± 0.95	9.23 ± 0.52	18.24 ± 0.32	20.05 ± 0.95	21.1 ± 0.5	20 ± 0.46	20.3 ± 0.52	21.3 ± 0.49	**21.85 ± 0.85**
4%	19.99 ± 1.04	11.52 ± 1.16	23.82 ± 0.86	22.97 ± 1.04	24.5 ± 0.47	23.2 ± 0.44	23.9 ± 0.5	24.1 ± 0.46	**24.01 ± 0.24**
5%	22.41 ± 0.54	13.66 ± 1.35	26.38 ± 0.85	24.37 ± 0.54	27.8 ± 0.44	26.1 ± 0.41	27.1 ± 0.44	28.4 ± 0.43	**27.26 ± 0.83**
6%	23.66 ± 0.49	15.49 ± 0.92	28.16 ± 0.62	26.93 ± 0.49	29.9 ± 0.4	28.4 ± 0.39	29.4 ± 0.4	30.8 ± 0.4	**31.24 ± 0.19**
7%	28.36 ± 0.85	18.52 ± 0.56	30.95 ± 0.66	27.37 ± 0.85	32 ± 0.38	30.3 ± 0.36	31.5 ± 0.38	31.7 ± 0.37	**32.37 ± 0.71**
8%	30.75 ± 1.12	18.52 ± 0.39	31.84 ± 0.23	28.32 ± 1.12	33.2 ± 0.36	31.6 ± 0.34	32.6 ± 0.36	32.9 ± 0.35	**33.31 ± 0.68**
9%	32.12 ± 1.48	18.52 ± 0.98	32.79 ± 0.94	29.19 ± 1.48	34.4 ± 0.34	33 ± 0.33	33.8 ± 0.35	34.1 ± 0.34	**34.04 ± 0.74**
10%	32.75 ± 1.02	19.54 ± 0.85	33.04 ± 0.65	31.02 ± 1.02	35.8 ± 0.32	34.2 ± 0.31	35 ± 0.33	35.4 ± 0.32	**35.81 ± 0.21**
20%	35.63 ± 0.99	35.14 ± 1.06	37.12 ± 0.85	35.24 ± 0.81	39.6 ± 0.28	38.7 ± 0.27	40.1 ± 0.29	41.2 ± 0.28	**39.15 ± 0.57**
50%	43.17 ± 1.02	44.14 ± 0.4	45.78 ± 0.41	42.18 ± 0.69	47.2 ± 0.24	46 ± 0.23	48.3 ± 0.25	49 ± 0.24	**46.18 ± 0.13**
75%	63.21 ± 0.5	66.12 ± 0.46	66.12 ± 0.61	63.05 ± 0.41	65.8 ± 0.2	65.1 ± 0.19	66.9 ± 0.21	67.8 ± 0.2	**68.01 ± 0.82**

Table 3: Performance (top-1 accuracy) of optimization and training property-based coreset methods on CIFAR100 trainsplit. The coresets were selected and finetuned on ResNet-18. The full trainset performance was $\mathbf{70.95 \pm 0.68}$. The mean accuracy over 5 runs, along with their standard deviation, is reported.

Coreset Sizes	Random	CRAIG	Glister	GraphCut	SloCurv	TDDS	Dyn − Unc	DUAL	**CLD (Ours)**
0.2%	3.66 ± 0.41	3.5 ± 0.42	3.43 ± 0.32	5.8 ± 0.24	3.62 ± 0.44	3.7 ± 0.44	2.1 ± 0.55	2 ± 0.56	**5.67 ± 0.36**
0.4%	6.03 ± 0.28	5.8 ± 0.4	4.91 ± 0.37	7.07 ± 0.39	5.46 ± 0.36	6 ± 0.41	3.5 ± 0.5	3.4 ± 0.52	**7.51 ± 0.59**
0.6%	6.8 ± 0.27	7.9 ± 0.39	7.49 ± 0.61	8.96 ± 0.31	7.44 ± 0.2	8.2 ± 0.4	5.1 ± 0.48	5 ± 0.49	**8.91 ± 0.41**
0.8%	7.96 ± 0.79	9.8 ± 0.47	8.65 ± 0.47	9.39 ± 0.81	9.96 ± 0.42	10.1 ± 0.48	7 ± 0.53	7.2 ± 0.54	**10.56 ± 0.24**
1%	9.38 ± 0.41	12.2 ± 0.44	9.04 ± 0.43	11.86 ± 0.47	12.17 ± 0.3	12.8 ± 0.45	9.5 ± 0.5	10.4 ± 0.51	**13.04 ± 0.54**
2%	12.74 ± 0.28	15.9 ± 0.42	14.54 ± 0.41	16.95 ± 0.55	13.35 ± 0.42	16.5 ± 0.43	14.2 ± 0.47	15.8 ± 0.48	**17.05 ± 0.22**
3%	16.58 ± 0.95	19.6 ± 0.46	17.47 ± 0.32	19.21 ± 0.57	22.67 ± 0.8	20.3 ± 0.47	18.9 ± 0.5	20.5 ± 0.5	**21.85 ± 0.85**
4%	19.99 ± 1.04	23 ± 0.44	23.99 ± 0.58	21.33 ± 0.71	21.97 ± 0.55	23.7 ± 0.45	22.7 ± 0.48	24.3 ± 0.47	**24.01 ± 0.24**
5%	22.41 ± 0.54	25.8 ± 0.4	24.83 ± 0.73	26.31 ± 0.58	23.44 ± 0.71	26.6 ± 0.42	25.8 ± 0.44	27.5 ± 0.43	**27.26 ± 0.83**
6%	23.66 ± 0.49	28.1 ± 0.38	26.57 ± 0.69	30.35 ± 0.68	25.41 ± 0.43	28.9 ± 0.39	28.2 ± 0.41	30 ± 0.4	**31.24 ± 0.19**
7%	28.36 ± 0.85	30 ± 0.36	27.57 ± 0.84	31.63 ± 0.71	27.45 ± 0.6	30.8 ± 0.37	30.3 ± 0.38	32.1 ± 0.38	**32.37 ± 0.71**
8%	30.75 ± 1.12	31.3 ± 0.34	28.79 ± 0.8	32.22 ± 0.48	29.17 ± 0.47	32 ± 0.35	31.7 ± 0.36	33.4 ± 0.35	**33.31 ± 0.68**
9%	32.12 ± 1.48	32.7 ± 0.32	30.22 ± 0.32	33.02 ± 0.83	30.71 ± 0.57	33.4 ± 0.33	33 ± 0.34	34.8 ± 0.33	**34.04 ± 0.74**
10%	32.75 ± 1.02	34.1 ± 0.3	31.22 ± 1.33	34.41 ± 0.96	33.17 ± 1.16	34.7 ± 0.31	34.4 ± 0.32	36.2 ± 0.31	**35.81 ± 0.21**
20%	35.63 ± 0.99	38.2 ± 0.26	36.49 ± 0.47	38.02 ± 0.52	37.23 ± 0.81	39.1 ± 0.27	38.8 ± 0.28	40.5 ± 0.27	**39.15 ± 0.57**
50%	43.17 ± 1.02	45.6 ± 0.22	41.81 ± 0.88	45.23 ± 0.42	45.19 ± 0.42	46.5 ± 0.23	45.8 ± 0.24	47.5 ± 0.23	**46.18 ± 0.13**
75%	63.21 ± 0.5	64.8 ± 0.19	63.85 ± 1.02	65.18 ± 0.32	66.53 ± 0.61	65.9 ± 0.2	64.5 ± 0.2	66.2 ± 0.19	**68.01 ± 0.82**

Table 4: Performance (top-1 accuracy) of score-based coreset methods on ImageNet-1k trainsplit. The coresets were selected and finetuned on ResNet-18. The full trainset performance was $\mathbf{69.91 \pm 0.01}$. The mean accuracy over 5 runs, along with their standard deviation, is reported.

Coreset Sizes	Random	Herding	Forgetting	Cal	EL2N	Moderate	CCS(AUM)	$\mathbb{D}^2$-Pruning	**CLD**
0.1%	0.7 ± 0.03	0.31 ± 0.01	0.64 ± 0.01	1.13 ± 0.12	0.88 ± 0.25	0.85 ± 0.2	1.52 ± 0.5	1.95 ± 0.4	**1.96 ± 0.7**
0.5%	3.98 ± 0.19	1.39 ± 0.17	4.78 ± 1.01	6.84 ± 0.13	5.83 ± 0.1	4.75 ± 0.5	7.04 ± 0.1	7.2 ± 0.25	**7.16 ± 0.63**
1%	7.86 ± 0.43	4.32 ± 0.62	12.67 ± 0.51	13.17 ± 0.22	15.2 ± 0.5	14.32 ± 1.03	14.86 ± 0.25	16.01 ± 0.4	**15.92 ± 0.41**
5%	39.78 ± 0.23	15.36 ± 0.18	44.86 ± 0.74	37.65 ± 1.3	40.43 ± 0.03	38.95 ± 0.25	44.04 ± 0.1	45.75 ± 0.5	**46.5 ± 0.19**
10%	51.24 ± 0.04	26.84 ± 0.05	53.19 ± 0.06	44.16 ± 0.78	45.16 ± 0.4	44.56 ± 0.1	52.01 ± 0.2	50.65 ± 0.3	**53.81 ± 0.23**
30%	60.87 ± 0.13	46.61 ± 0.87	60.9 ± 0.05	54.41 ± 0.45	53.22 ± 0.25	55.29 ± 0.1	61.84 ± 0.5	60.75 ± 0.1	**62.91 ± 0.51**
40%	62.13 ± 0.38	53.88 ± 0.23	62.39 ± 0.91	58.45 ± 0.92	56.45 ± 0.1	60.08 ± 0.15	62.48 ± 0.02	61.04 ± 0.5	**63.51 ± 0.75**
50%	64.11 ± 0.12	59.14 ± 0.41	63.18 ± 0.05	60.11 ± 0.6	59.46 ± 0.45	62.58 ± 0.25	64.31 ± 0.04	64.92 ± 0.65	**65.78 ± 1.03**
65%	65.21 ± 0.03	64.23 ± 0.2	65.24 ± 0.02	64.42 ± 0.01	61.28 ± 0.25	64.98 ± 0.1	65.17 ± 0.1	67.01 ± 0.1	**68.02 ± 0.38**
70%	68.81 ± 0.04	65.22 ± 0.02	67.85 ± 0.9	66.57 ± 0.03	64.23 ± 0.89	65.18 ± 0.03	68.81 ± 0.1	68.91 ± 0.01	**68.91 ± 0.01**
75%	68.41 ± 0.02	67.42 ± 0.01	68.01 ± 0.1	67.12 ± 0.02	65.45 ± 0.2	67.13 ± 0.03	69.01 ± 0.03	69.42 ± 0.05	**69.42 ± 0.05**
80%	68.12 ± 0.03	68.02 ± 0.02	68.81 ± 0.5	68.15 ± 0.03	66.95 ± 0.25	68.9 ± 0.01	69.93 ± 0.02	69.93 ± 0.02	**69.93 ± 0.02**
85%	68.75 ± 0.05	68.01 ± 0.03	68.81 ± 0.5	68.91 ± 0.04	67.17 ± 0.1	68.9 ± 0.2	69.91 ± 0.25	69.93 ± 0.02	**69.93 ± 0.02**
90%	69.1 ± 0.78	69.92 ± 0.4	70.04 ± 0.52	69.23 ± 0.5	68.81 ± 0.3	69.01 ± 0.2	70.12 ± 0.03	70.12 ± 0.03	**70.12 ± 0.03**
95%	69.91 ± 0.06	69.91 ± 0.04	69.91 ± 0.04	70.12 ± 0.01	69.91 ± 0.04	70.12 ± 0.03	69.91 ± 0.1	70.12 ± 0.03	**70.12 ± 0.03**

Table 5: Performance (top-1 accuracy) of optimization and training property-based coreset methods on ImageNet-1k trainsplit. The coresets were selected and finetuned on ResNet-18. The full trainset performance was $\mathbf{69.91 \pm 0.01}$. The mean accuracy over 5 runs, along with their standard deviation, is reported.

Coreset Sizes	Random	CRAIG	Glister	GraphCut	SloCurv	TDDS	Dyn − Unc	DUAL	**CLD**
0.1%	0.7 ± 0.03	0.94 ± 0.1	0.86 ± 0.01	1.09 ± 0.09	1.23 ± 0.06	1.04 ± 0.2	0.45 ± 0.9	0.41 ± 1.06	**1.96 ± 0.7**
0.5%	3.98 ± 0.19	6.41 ± 0.25	5.55 ± 0.05	7.27 ± 0.03	5.89 ± 0.07	5.64 ± 0.03	1.45 ± 1.05	1.34 ± 0.87	**7.16 ± 0.63**
1%	7.86 ± 0.43	15.56 ± 0.05	12.45 ± 0.01	14.27 ± 0.31	14.17 ± 0.02	14.05 ± 0.1	3.92 ± 0.8	4.85 ± 0.75	**15.92 ± 0.41**
5%	39.78 ± 0.23	39.95 ± 0.01	42.19 ± 0.03	39.8 ± 0.6	40.1 ± 0.14	40.54 ± 0.05	15.98 ± 0.5	16.2 ± 0.4	**46.5 ± 0.19**
10%	51.24 ± 0.04	46.76 ± 0.1	50.1 ± 0.01	48.27 ± 1.02	46.39 ± 0.5	46.45 ± 0.25	29.78 ± 0.6	50.75 ± 0.5	**53.81 ± 0.23**
30%	60.87 ± 0.13	55.41 ± 0.05	58.53 ± 0.05	61.23 ± 0.01	57.19 ± 0.01	57.24 ± 0.1	50.16 ± 0.5	60.19 ± 0.03	**62.91 ± 0.51**
40%	62.13 ± 0.38	56.55 ± 0.02	61.72 ± 0.02	63.23 ± 0.08	62.11 ± 0.67	62.23 ± 0.5	60.25 ± 0.2	63.45 ± 0.25	**63.51 ± 0.75**
50%	64.11 ± 0.12	58.56 ± 0.5	63.41 ± 0.51	65.17 ± 0.05	64.78 ± 0.13	63.96 ± 0.81	63.17 ± 0.1	65.21 ± 0.04	**65.78 ± 1.03**
65%	65.21 ± 0.03	63.41 ± 0.2	65.83 ± 0.02	67.91 ± 0.54	65.81 ± 0.02	65.19 ± 0.1	65.98 ± 0.25	68.31 ± 0.01	**68.02 ± 0.38**
70%	68.81 ± 0.04	65.21 ± 0.01	67.91 ± 0.03	68.52 ± 0.04	67.18 ± 0.03	67.25 ± 0.01	66.32 ± 0.1	68.76 ± 0.5	**68.91 ± 0.01**
75%	68.41 ± 0.02	68.01 ± 0.5	68.54 ± 0.46	68.81 ± 0.02	68.03 ± 0.15	68.14 ± 0.25	68.19 ± 0.01	69.92 ± 0.01	**69.42 ± 0.05**
80%	68.12 ± 0.03	68.01 ± 0.5	68.78 ± 0.02	69.12 ± 0.05	69.1 ± 0.14	68.91 ± 0.2	68.19 ± 0.01	69.92 ± 0.01	**69.93 ± 0.02**
85%	68.75 ± 0.05	68.78 ± 0.02	68.78 ± 0.02	70.01 ± 0.28	69.1 ± 0.02	68.91 ± 0.25	69.93 ± 0.2	69.93 ± 0.2	**69.93 ± 0.02**
90%	69.1 ± 0.78	68.48 ± 0.25	69.18 ± 0.34	70.12 ± 0.43	69.68 ± 0.03	69.68 ± 0.03	70.12 ± 0.03	70.12 ± 0.03	**70.12 ± 0.03**
95%	69.91 ± 0.06	69.91 ± 0.04	69.91 ± 0.04	70.12 ± 0.43	69.91 ± 0.04	69.68 ± 0.03	70.12 ± 0.03	70.12 ± 0.03	**70.12 ± 0.03**

Table 6: Cross-architecture performance of coresets of different sizes of ImageNet-1k identified by CLD. Each cell reports mean test accuracy (top) and standard deviation (bottom) over 5 runs. Minimal accuracy drop (< 1%) is observed when transferring coresets from a smaller ResNet-18 model to larger or different architectures.

Target Model	Source Model	Coreset size (% of dataset)							
		5%	10%	25%	40%	50%	75%	80%	100%
ResNet-34	ResNet-18	46.91 ± 0.03	54.83 ± 0.05	60.21 ± 0.12	66.83 ± 0.48	68.93 ± 0.01	71.12 ± 0.01	73.04 ± 0.05	73.21 ± 0.01
ResNet-34	ResNet-34	47.01 ± 0.02	54.75 ± 0.35	60.98 ± 0.71	67.26 ± 0.10	69.03 ± 0.04	71.06 ± 0.02	73.04 ± 0.01	73.21 ± 0.01
ResNet-50	ResNet-18	47.19 ± 0.01	56.14 ± 0.05	62.83 ± 0.13	68.14 ± 0.01	71.15 ± 0.03	73.04 ± 0.07	74.95 ± 0.02	75.81 ± 0.05
ResNet-50	ResNet-50	48.10 ± 0.05	57.03 ± 0.03	63.14 ± 0.02	68.91 ± 0.05	71.25 ± 0.04	73.57 ± 0.01	74.95 ± 0.02	75.81 ± 0.05
DenseNet-121	ResNet-18	45.18 ± 0.37	55.18 ± 0.61	61.19 ± 0.01	67.34 ± 0.04	71.02 ± 0.83	71.85 ± 0.04	73.85 ± 0.02	74.90 ± 0.37
DenseNet-121	DenseNet-121	46.07 ± 0.02	55.88 ± 0.03	62.01 ± 0.72	67.91 ± 0.61	71.36 ± 0.10	72.18 ± 0.07	74.04 ± 0.04	74.90 ± 0.37
VGG-19(bn)	ResNet-18	43.12 ± 0.04	53.18 ± 0.03	60.12 ± 0.02	66.17 ± 0.07	70.37 ± 0.01	72.01 ± 0.04	73.98 ± 0.37	74.70 ± 0.71
VGG-19(bn)	VGG-19(bn)	44.01 ± 0.50	54.12 ± 0.47	61.01 ± 0.31	67.09 ± 0.16	70.25 ± 0.25	72.58 ± 0.02	74.05 ± 0.04	74.70 ± 0.71

D Additional Ablations

D.1 Stability across random seeds

We measure sensitivity to random initialization by computing per-example CLD scores across five independent seeds on ImageNet-1k (ResNet-18). The pairwise mean absolute error (MAE) between score vectors is consistently below 10^{-5}, indicating negligible variance and high reproducibility; see Figure 7a.

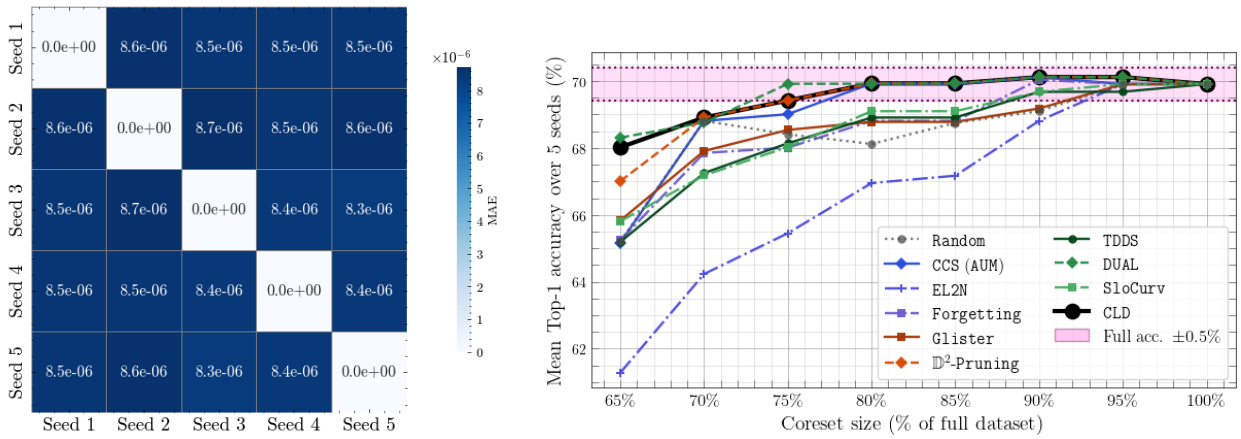

(a) **Seed reproducibility.** Pairwise MAE of CLD scores across 5 seeds (lower is better).

(b) **Subset size vs. accuracy.** ImageNet-1k, ResNet-18. The shaded band marks the 0.5% tolerance below full-data accuracy.

Figure 7: Seed-wise stability and subset-size trade-offs on ImageNet-1k.

D.2 Minimum subset size for full-data accuracy

We quantify the subset fraction required to recover near full-data performance on ImageNet-1k (ResNet-18). As shown in Figure 7b, `CLD` attains test accuracy within 0.5% of the full-data model using only 75% of the training set, on par with $\mathbb{D}^2$-`Pruning` and `DUAL`, and superior to other baselines we evaluated.

E Detailed Explanation of Compute and Storage Cost of Coreset Methodologies

Recap of Notation We denote the number of training samples by N ($\mathbf{S} \sim \mathbf{D}^N$) and the number of query (held-out validation) samples by Q ($\mathbf{V} \sim \mathbf{D}^Q$). The model is trained for T epochs. Certain TDA metrics have hyperparameters (denoted λ_τ) used to compute the TDA metric τ, which may influence computational cost.

We measure computation in floating-point operations (FLOPs). Let f_{large} be the cost of a *single-example* forward pass for the large model with p_{large} parameters, and approximate the backward-pass cost as $2f_{\text{large}}$. When a proxy (smaller) model is used, we write its per-example forward cost and parameter count as f and p, with $f \ll f_{\text{large}}$ and $p \ll p_{\text{large}}$.

R is the number of model retrainings (when applicable). k is the coreset size; d is the feature dimensionality; and B is the minibatch size (used during training but not appearing in per-example FLOP counts). Some methods perform subset *reselection* during training; when used, we denote the reselection interval (in epochs) by γ.

Reference: full-data training (large model) Training the large model on all N points for T epochs costs $3NT\, f_{\text{large}}$ FLOPs and stores p_{large} parameters (ignoring optimizer state). Totals below are the end-to-end cost to (i) select a coreset of size k and (ii) train the large model on that coreset.

Example scenario (used for all plug-in estimates). To further illustrate the computational efficiency of `CLD`, we provide approximate cost values by substituting the values of the parameters for finding and training a 10% coreset on the ImageNet-1k dataset.

- N=1,268,355 (99% of train), Q=12,812 (remaining 1%), d=224×224×3, c=1000.
- Size of coreset k=126,836.
- Proxy encoder: ResNet-18 with p=11,689,128 and per-example forward FLOPs f=1,818,228,160.
- Large model: ResNet-50 with p_{large}=25,557,032 and $f_{\text{large}}\approx$8,178,000,000.
- We use the standard ImageNet recipe of T=T_{proxy}=90 epochs (Yang, 2017).
- When a method has additional parameters, we use the paper's choice (e.g., in `Glister`, γ=20).

E.1 Score-based Methods

E.1.1 Kernel Herding (`Herding`)

`Herding` (Chen et al., 2010) iteratively constructs a representative subset by approximating the data distribution in an RKHS. At iteration t, it selects

$$\vec{z}^{*t} \;=\; \arg\max_{\vec{z}\in\mathbf{S}} \langle w_{t-1},\, \phi(\vec{z})\rangle,$$

where $\phi(\cdot)$ is the kernel feature map and w_{t-1} is an RKHS weight vector. Repeating for k iterations yields a size-k coreset.

Execution. One-time selection prior to training the large model (a proxy encoder is used to obtain features):

i) *Train proxy encoder:* train a proxy model for T_{proxy} epochs (forward cost f, parameters p).
ii) *Encode full dataset:* extract features for all N points using the trained proxy (Nf FLOPs).
iii) *Herding selection:* for t=1:k, update candidate scores and select $\vec{z}^{*t}$ using inner products in feature space (explicit features of dim. d give $\mathcal{O}(Nd)$ per iteration, i.e., $\mathcal{O}(Ndk)$ total).
iv) *Train on coreset:* train the large model on the selected k points for T_{late} epochs (here T_{late}=T).

End-to-end compute (selection + coreset training).

$$\boxed{\text{Compute}_{\texttt{Herding}} = \underbrace{3N\,T_{\text{proxy}}\,f}_{\text{train proxy}} + \underbrace{Nf}_{\text{feature extraction}} + \underbrace{\mathcal{O}(Ndk)}_{\text{iterative herding updates}} + \underbrace{3k\,T_{\text{late}}\,f_{\text{large}}}_{\text{train large on coreset}}}$$

Selection-stage storage overhead. Storing explicit features dominates; caching a $k\times k$ Gram among selected points is optional:

$$\boxed{\text{StorageOverhead}_{\texttt{Herding}} = \ \mathcal{O}(Nd)\ \ (+\,\mathcal{O}(k^2)\text{ optional Gram})}$$

Example scenario values (ImageNet-1k; $T_{\textbf{late}}$=90, $T_{\textbf{proxy}}$=90).

$$\text{Compute}_{\texttt{Herding}}\ (\text{PFLOPs only}) \approx \underbrace{622.663}_{3NT_{\text{proxy}}f} + \underbrace{2.306}_{Nf} + \underbrace{280.061}_{3kT_{\text{late}}\,f_{\text{large}}} = \textbf{905.031}\ \text{PFLOPs},$$

(negligible herding updates)

$$\text{StorageOverhead}_{\texttt{Herding}}(\text{float32}) \approx Nd \times 4 = \textbf{763.692}\ \text{GB (features only)}.$$

E.1.2 Example Forgetting (`Forgetting`)

`Forgetting` (Toneva et al., 2018) measures, for each training sample, how many times it transitions from being correctly classified to incorrectly classified during training ("forgetting events"). Examples with higher forgetting counts are ranked as more informative.

Execution. One-time selection prior to training the large model on the coreset. Let T_{early} be the number of early epochs run on the full dataset to collect forgetting statistics, and $T_{\text{late}} = T - T_{\text{early}}$ the remaining epochs used to train on the selected coreset:

i) Train on all N points for T_{early} epochs while tracking, per example, the previous correctness bit and a forgetting counter (constant-time update per visit).
ii) Select the top k examples by forgetting count; train the large model on this coreset for T_{late} epochs.

End-to-end compute (selection + coreset training).

$$\boxed{\text{Compute}_{\texttt{Forgetting}} = \underbrace{3N\,T_{\text{early}}\,f_{\text{large}}}_{\text{collect forgetting on full data}} + \underbrace{3k\,T_{\text{late}}\,f_{\text{large}}}_{\text{train large on coreset}}}$$

Selection-stage storage overhead. Streaming the metric requires only one scalar counter (and one correctness bit) per training example:

$$\boxed{\text{StorageOverhead}_{\texttt{Forgetting}} = \ \mathcal{O}(N)\ \ (\text{per-sample counter/bit})}$$

Example scenario values (ImageNet-1k; $T_{\textbf{early}}$=10, $T_{\textbf{late}}$=80).

$$\text{Compute}_{\texttt{Forgetting}}\ (\text{PFLOPs only}) \approx \underbrace{311.178}_{3NT_{\text{early}}\,f_{\text{large}}} + \underbrace{248.943}_{3kT_{\text{late}}\,f_{\text{large}}} = \textbf{560.122}\ \text{PFLOPs},$$

$$\text{StorageOverhead}_{\texttt{Forgetting}}(\text{float32}) \approx N \times 4 = 5{,}073{,}420\ \text{B} = \textbf{0.005}\ \text{GB}.$$

E.1.3 Area Under Margin (`AUM`)

`AUM` (Pleiss et al., 2020) scores each training sample by aggregating its *margin* over training (e.g., logit of the true class minus the max non-true logit), producing the *area under the margin* across epochs/updates. Higher absolute AUM indicates more consistently confident predictions; lower AUM can flag ambiguous or noisy samples. We compute AUM with a *proxy* model and then train the large model on the selected coreset.

Execution. One-time selection with a proxy; the large model then trains on the coreset for all T epochs:

i) *Train proxy & log margins:* train a proxy for T_{proxy} epochs on all N samples (per-example forward cost f, parameters p), recording each sample's margin as it appears in training (no extra forward/backward beyond training).
ii) *Compute AUM & select:* for each sample, aggregate (e.g., sum/average) its logged margins to obtain AUM and select a size-k coreset according to the desired criterion (e.g., highest AUM, or filter low-AUM points).
iii) *Train large on coreset:* train the large model on the selected k samples for T epochs.

End-to-end compute (selection + coreset training).

$$\boxed{\text{Compute}_{\texttt{AUM}} = \underbrace{3N\,T_{\text{proxy}}\,f}_{\text{train proxy (margin logging piggybacks)}} + \underbrace{3k\,T\,f_{\text{large}}}_{\text{train large on coreset}}}$$

Selection-stage storage overhead. AUM can be streamed with a running sum/count per sample:

$$\boxed{\text{StorageOverhead}_{\texttt{AUM}} = \ \mathcal{O}(N)\ \ \text{(running sums)}}$$

Example scenario values (ImageNet-1k; T_{proxy}=90, T=90).

$$\text{Compute}_{\texttt{AUM}}\ \text{(PFLOPs only)} \approx \underbrace{622.663}_{3NT_{\text{proxy}}f} + \underbrace{280.061}_{3kT\,f_{\text{large}}} = \mathbf{902.724}\ \text{PFLOPs},$$

$$\text{StorageOverhead}_{\texttt{AUM}}\ \text{(float32)} \approx N \times 4 = 5{,}073{,}420\ \text{B} = \mathbf{0.005}\ \text{GB}.$$

E.1.4 Contrastive Active Learning (`Cal`)

`Cal` (Margatina et al., 2021) acquires unlabeled examples that are near labeled ones in feature space yet differ in predictive probabilities (contrastive pairs), using nearest neighbors over encoder features and a simple divergence-based ranking.

Execution. A one-time selection stage is performed prior to training the large model:

i) train a *proxy* model from scratch on the (growing) labeled set up to size k (per-example forward cost $f \ll f_{\text{large}}$);
ii) encode all U unlabeled points with the trained proxy (here U=N);
iii) run kNN-style neighbor search between the unlabeled pool and the labeled set (size k), and select a coreset of size k.

(The divergence computation is much cheaper than (ii)–(iii) and is absorbed into big-$\mathcal{O}$.)

Overall compute (select once, then train-on-coreset).

$$\boxed{\text{Compute}_{\texttt{Cal}} = \underbrace{3k\,T_{\text{proxy}}\,f}_{\text{train proxy}} + \underbrace{Uf}_{\text{encode unlabeled pool}} + \underbrace{\mathcal{O}(U\,k\,d)}_{k\text{NN over features}} + \underbrace{3kT\,f_{\text{large}}}_{\text{train large on coreset}}}$$

Selection-stage storage overhead. Storage overhead is due to the cached features for the unlabeled pool

$$\boxed{\text{StorageOverhead}_{\texttt{Cal}} = \ \mathcal{O}(Ud)\ \ \text{(proxy features)}}$$

Example scenario values: ImageNet-1k; U=N).

$$\begin{aligned}\text{Compute}_{\texttt{Cal}}\ \text{(PFLOPs only)} &\approx \underbrace{62.267}_{3kT_{\text{proxy}}f} + \underbrace{2.306}_{Uf\ \ (U=N)} + \underbrace{280.061}_{3kT\,f_{\text{large}}} \\ &= \mathbf{344.634}\ \text{PFLOPs},\end{aligned}$$

$$\text{StorageOverhead}_{\texttt{Cal}}\ \text{(float32)} \approx Ud \times 4 = \ \mathbf{763.739}\ \text{GB}.$$

E.1.5 Gradient and Error L2 Norm-based Data Pruning (`GraNd`, `EL2N`)

`GraNd` (Paul et al., 2021) ranks training examples by the (expected) per-example gradient norm early in training:

$$\mathrm{GraNd}_t(\vec{z}_m) = \mathbb{E}_{\theta_t}\left\|\nabla_{\theta_t}\,\ell(\theta_t, \vec{z}_m)\right\|_2^2,$$

averaged over multiple random initializations and early epochs, then retains the top-k examples.

`EL2N` (Paul et al., 2021) ranks examples by the (expected) L2 error of predictions early in training:

$$\mathrm{EL2N}_t(\vec{z}_m) = \mathbb{E}_{\theta_t}\left\|\mathbf{p}_\theta(\vec{x}_m) - \mathbf{y}_m\right\|_2,$$

where $\mathbf{p}_\theta$ are class probabilities and $\mathbf{y}_m$ is the one-hot label. Scores are computed at small t and optionally averaged over R runs.

Execution. One-time selection prior to training the large model. Let T_{early} be the number of early epochs used for scoring and $T_{\text{late}} = T - T_{\text{early}}$ the remaining epochs used to train on the coreset:

i) For each of R initializations, train on all N points for T_{early} epochs (costing $3NT_{\text{early}}f_{\text{large}}$) while logging per-example predictions.
   (a) `EL2N`: compute scores directly from the logged predictions (no extra passes).
   (b) `GraNd`: run an *additional scoring sweep* to obtain per-sample gradients (one forward + one backward pass per example per early epoch).

ii) Average scores across runs; keep the top k; train the large model on the coreset for T_{late} epochs.

End-to-end compute (selection + train-on-coreset).

$$\boxed{\begin{aligned}\text{Compute}_{\texttt{EL2N}} &= \underbrace{3N\,T_{\text{early}}\,R\,f_{\text{large}}}_{\text{early training (errors reused)}} + \underbrace{3k\,T_{\text{late}}\,f_{\text{large}}}_{\text{train large on coreset}},\\ \text{Compute}_{\texttt{GraNd}} &= \underbrace{3N\,T_{\text{early}}\,R\,f_{\text{large}}}_{\text{early training}} + \underbrace{3N\,T_{\text{early}}\,R\,f_{\text{large}}}_{\text{extra per-sample gradient sweeps}} + \underbrace{3k\,T_{\text{late}}\,f_{\text{large}}}_{\text{train large on coreset}}.\end{aligned}}$$

Selection-stage storage overhead. During scoring, a running vector of N scalar scores need to be stored:

$$\boxed{\begin{aligned}\text{StorageOverhead}_{\texttt{EL2N}} &= \mathcal{O}(N),\\ \text{StorageOverhead}_{\texttt{GraNd}} &= \mathcal{O}(N).\end{aligned}}$$

Example scenario values (ImageNet-1k; R=10, T_{early}=10, T_{late}=80).

$$\text{Compute}_{\texttt{EL2N}}\ (\text{PFLOPs only}) \approx \underbrace{3{,}111.782}_{3NT_{\text{early}}R\,f_{\text{large}}} + \underbrace{248.943}_{3kT_{\text{late}}\,f_{\text{large}}} = \mathbf{3{,}360.725}\ \text{PFLOPs},$$

$$\text{Compute}_{\texttt{GraNd}}\ (\text{PFLOPs only}) \approx \underbrace{3{,}111.782}_{\text{early training}} + \underbrace{3{,}111.782}_{\text{extra gradient sweeps}} + \underbrace{248.943}_{3kT_{\text{late}}\,f_{\text{large}}} = \mathbf{6{,}472.507}\ \text{PFLOPs},$$

$$\text{StorageOverhead (float32)} \approx N \times 4 = \mathbf{0.005}\ \text{GB for each.}$$

E.1.6 Using Class Feature Medians (`Moderate`)

`Moderate` (Xia et al., 2022) builds a representative coreset by selecting, *within each class*, the samples whose feature-to-center distances are closest to that class's *median* distance (thus avoiding both easy near-center redundancies and far-out outliers). We compute class centers and distances in a proxy feature space.

Execution. One-time selection with a proxy, then train the large model on the coreset for all T epochs:

i) *Train proxy:* train a proxy encoder on all N samples for T_{proxy} epochs (per-example forward cost f, parameters p).
ii) *Encode dataset:* extract proxy features for all N samples (cost Nf FLOPs).
iii) *Class-median selection:* for each class, compute the class center and all sample distances, then select the per-class quota of samples whose distances are closest to the class-wise median (distance computation $\mathcal{O}(Nd)$; median/quantile selection $\mathcal{O}(N \log N)$ or linear-time selection).
iv) *Train large on coreset:* train the large model on the selected k samples for T epochs.

End-to-end compute (selection + coreset training).

$$\boxed{\text{Compute}_{\texttt{Moderate}} = \underbrace{3N\,T_{\text{proxy}}\,f}_{\text{train proxy}} + \underbrace{Nf}_{\text{feature extraction}} + \underbrace{\mathcal{O}\big(Nd + N\log N\big)}_{\text{class centers, distances, medians}} + \underbrace{3k\,T\,f_{\text{large}}}_{\text{train large on coreset}}}$$

Selection-stage storage overhead. The main storage overhead is from caching the features during selection

$$\boxed{\text{StorageOverhead}_{\texttt{Moderate}} = \ \mathcal{O}(Nd) \ \ \text{(proxy features)}}$$

Example scenario values (ImageNet-1k; T_{proxy}=90, T=90).

$$\text{Compute}_{\texttt{Moderate}}\ \text{(PFLOPs only)} \approx \underbrace{622.663}_{3NT_{\text{proxy}}f} + \underbrace{2.306}_{Nf} + \underbrace{280.061}_{3kT\,f_{\text{large}}} = \textbf{905.031}\ \text{PFLOPs},$$

$$\text{StorageOverhead}_{\texttt{Moderate}}(\text{float32}) \approx Nd \times 4 = \ \textbf{763.739}\ \text{GB}.$$

E.1.7 Message Passing ($\mathbb{D}^2 - \texttt{Pruning}$)

$\mathbb{D}^2$`Pruning` (Maharana et al., 2024) selects a coreset by *balancing difficulty and diversity* via message passing on a dataset graph built from proxy features. Initial per-sample difficulty scores (from the proxy) are diffused over a kNN graph so that each example's score incorporates information from its neighbors; a graph-based sampler then selects a subset that covers diverse yet difficult regions.

Execution. One-time selection with a proxy, then train the large model on the coreset for all T epochs:

i) *Train proxy:* train a proxy encoder on all N samples for T_{proxy} epochs (per-example forward cost f, parameters p).
ii) *Encode dataset:* extract proxy features for all N samples (cost Nf FLOPs).
iii) *Build graph:* construct a kNN graph over the features (e.g., ANN); cost $\mathcal{O}(N\,k\,d)$ (or $\mathcal{O}(N\,d\log N)$).
iv) *Message passing & sampling:* run H rounds of (forward/reverse) message passing on the $N \times k$ edges to update difficulty-aware scores, then sample a size-k coreset (cost $\mathcal{O}(H\,N\,k)$ plus linear-time sampling).
v) *Train large on coreset:* train the large model on the selected k samples for T epochs.

End-to-end compute (selection + coreset training).

$$\boxed{\text{Compute}_{\mathbb{D}^2\texttt{Pruning}} = \underbrace{3N\,T_{\text{proxy}}\,f}_{\text{train proxy}} + \underbrace{Nf}_{\text{feature extraction}} + \underbrace{\mathcal{O}(N\,k\,d) + \mathcal{O}(H\,N\,k)}_{\text{graph build \& message passing}} + \underbrace{3k\,T\,f_{\text{large}}}_{\text{train large on coreset}}}$$

Selection-stage storage overhead. Caching proxy features dominates; the kNN adjacency is linear in N and smaller in practice:

$$\boxed{\text{StorageOverhead}_{\mathbb{D}^2\texttt{Pruning}} = \ \mathcal{O}(Nd) \ + \ \mathcal{O}(N\kappa) \ \ \text{(features + } k\text{NN graph)}}$$

Example scenario values (ImageNet-1k; T_{proxy}=90, T=90).

$$\text{Compute}_{\mathbb{D}^2\texttt{Pruning}}\ \text{(PFLOPs only)} \approx \underbrace{622.663}_{3NT_{\text{proxy}}f} + \underbrace{2.306}_{Nf} + \underbrace{280.061}_{3kT\,f_{\text{large}}} = \textbf{905.031}\ \text{PFLOPs}, \quad \text{(excluding graph terms)}$$

$$\text{StorageOverhead}_{\mathbb{D}^2\texttt{Pruning}}\ (\text{float32}) \approx Nd \times 4 = \ \textbf{763.692}\ \text{GB}.$$

E.2 Optimization-based Methods

E.2.1 Gradient Matching Optimization (CRAIG)

CRAIG (Mirzasoleiman et al., 2020) selects a subset whose (aggregated) gradients closely match those of the full dataset across training, typically using a submodular (stochastic-greedy) objective over *per-sample gradient embeddings* at selected *anchor* epochs. We compute embeddings with a proxy model and then train the large model on the coreset for all T epochs.

Execution. One-time selection with a proxy, then train the large model:

i) *Train proxy:* train a proxy network on all N samples for T_{proxy} epochs (per-example forward cost f, parameters p).

ii) *Per-sample gradient embeddings at anchors:* every γ_{anc} epochs (anchors $A{=}T_{\text{proxy}}/\gamma_{\text{anc}}$), compute for each sample the *last-layer* gradient embedding using only forward-pass outputs:

$$g_i^{(a)} \;=\; \big(\mathbf{p}_\theta^{(a)}(\vec{x}_i) - \mathbf{y}_i\big) \;\oplus\; h_\theta^{(a)}(\vec{x}_i),$$

where h_θ is the penultimate representation (dim. F) and $\mathbf{p}_\theta - \mathbf{y}_i \in \mathbb{R}^C$ is the class-probability error; this avoids backward passes (piggybacks on training). Selection then runs stochastic-greedy on these embeddings per anchor.

iii) *Select & train large:* union the anchor-wise selections to a size-k coreset and train the large model on it for all T epochs.

End-to-end compute (selection + coreset training).

$$\text{Compute}_{\texttt{CRAIG}} = \underbrace{3N\,T_{\text{proxy}}\,f}_{\text{train proxy (embeddings piggyback)}} + \underbrace{\mathcal{O}\big(A\,(Nk + N\log(1/\epsilon))\,D_{\text{eff}}\big)}_{\text{stochastic-greedy over anchors}} + \underbrace{3k\,T\,f_{\text{large}}}_{\text{train large on coreset}}$$

Here $D_{\text{eff}} \approx F{+}C$ is the embedding dimensionality (penultimate features and class-probability error); the submodular arithmetic is negligible in FLOPs relative to training and is kept in big-$\mathcal{O}$.

Selection-stage storage overhead. We stream anchor processing so only a single anchor's embeddings need be cached at once:

$$\text{StorageOverhead}_{\texttt{CRAIG}} = \;\mathcal{O}\big(N(F{+}C)\big) \;\; \text{(per-anchor embeddings, streamed per anchor)}$$

Example scenario values (ImageNet-1k; $T_{\text{proxy}}{=}90$, $T{=}90$, $F{=}512$, $C{=}1000$).

$$\text{Compute}_{\texttt{CRAIG}}\ \text{(PFLOPs only; excluding big-}\mathcal{O}\text{ selection)} \approx \underbrace{622.663}_{3NT_{\text{proxy}}f} + \underbrace{280.061}_{3kT\,f_{\text{large}}} = \mathbf{902.724}\ \text{PFLOPs},$$

$$\text{Storage}_{\texttt{CRAIG}}\ (\text{float32}) \approx N(F{+}C)\times 4 \;=\; \mathbf{7.671}\ \text{GB}.$$

E.2.2 Generalization-based Data Subset Selection for Efficient and Robust Learning (Glister)

Glister (Killamsetty et al., 2021b) selects $\mathbf{S}_j$ of size k via a mixed discrete–continuous bi-level objective:

$$\underset{\mathbf{S}_j\subseteq\mathbf{S},\,|\mathbf{S}_j|\le k}{\arg\max}\ \mathcal{L}_{\mathbf{V}}\big(\theta^\star(\mathbf{S}_j)\big) \quad \text{where} \quad \theta^\star(\mathbf{S}_j) = \underset{\theta}{\arg\max}\ \mathcal{L}_{\mathbf{S}}(\theta;\mathbf{S}_j).$$

Execution. Glister *replaces the training loop*: it interleaves training on the current subset with periodic re-selection every γ epochs (using stochastic-greedy with a Taylor approximation).

Overall compute (train-on-coreset). Training on the coreset over T epochs costs $3kT\,f_{\text{large}}$. Selection across T epochs at frequency γ costs $\mathcal{O}\left(\frac{\left(kQ+N\log(1/\epsilon)\right)f_{\text{large}}\,T}{\gamma}\right)$. Hence

$$\text{Compute}_{\texttt{Glister}} = 3kT\,f_{\text{large}} + \mathcal{O}\left(\frac{\left(kQ + N\log(1/\epsilon)\right)f_{\text{large}}\,T}{\gamma}\right)$$

Selection-stage storage overhead. Storage overhead is from validation caches:

$$\boxed{\text{StorageOverhead}_{\texttt{Glister}} = \ \mathcal{O}(Q) \ \ \text{(validation cache)}}$$

Example scenario values:

$$\begin{aligned}\text{Compute}_{\texttt{Glister}} &\approx \underbrace{280.061}_{3kT\, f_{\text{large}}\ \text{(PFLOPs)}} + \underbrace{60{,}017.420}_{\frac{T}{\gamma}(kQ+N\log(1/\epsilon))\, f_{\text{large}}\ \text{(PFLOPs; } \epsilon=0.01,\ \gamma=20)} \\ &= \ \mathbf{60{,}297.481}\ \text{PFLOPs},\end{aligned}$$

$$\text{StorageOverhead}_{\texttt{Glister}} \approx Q \times 4 = 51{,}248\ \text{B} \approx \mathbf{5.1 \times 10^{-5}}\ \text{GB}\ (\approx 0.05\ \text{MB}).$$

E.2.3 GraphCut-based Data Subset Selection (`GraphCut`)

`GraphCut` (Iyer et al., 2021) selects $\mathbf{S}_j$ via the generalized graph-cut function

$$f(\mathbf{S}_j) = \lambda \sum_{m \in \mathbf{S}} \sum_{j \in \mathbf{S}_j} s(m, j) \ - \sum_{j_1, j_2 \in \mathbf{S}_j} s(j_1, j_2), \quad \lambda \geq 2.$$

Execution. `GraphCut` *adds* a one-time selection stage prior to training (it does not replace training). The procedure is:

i) train a proxy model;
ii) extract features for all N training points using the trained proxy (per-example cost $f \ll f_{\text{large}}$);
iii) run (stochastic-)greedy selection to build a size-k subset.

(Similarity operations are typically much cheaper than (ii)–(iii), so we absorb them into big-$\mathcal{O}$.)

Overall compute (train-on-coreset). One-time selection (including proxy training) + large-model training:

$$\boxed{\text{Compute}_{\texttt{GraphCut}} = \underbrace{3N\, T_{\text{proxy}}\, f}_{\text{train proxy}} + \underbrace{Nf}_{\text{feature extraction}} + \underbrace{\mathcal{O}(N^2 k)}_{\text{greedy selection}} + \underbrace{3kT\, f_{\text{large}}}_{\text{train large on coreset}}}$$

Selection-stage storage overhead. Storage overhead is from storing pairwise similarities

$$\boxed{\text{StorageOverhead}_{\texttt{GraphCut}} = \ \mathcal{O}(N^2) \ \ \text{(pairwise similarities / kernel)}}$$

Example scenario values:

$$\begin{aligned}\text{Compute}_{\texttt{GraphCut}}\ \text{(PFLOPs only)} &\approx \underbrace{622.663}_{3NT_{\text{proxy}}f} + \underbrace{2.306}_{Nf} + \underbrace{280.061}_{3kT\, f_{\text{large}}} \\ &= \ \mathbf{905.031}\ \text{PFLOPs},\end{aligned}$$

$$\begin{aligned}\text{StorageOverhead}_{\texttt{GraphCut}}\ \text{(float32)}: \ &\text{full kernel peak} \approx \mathbf{6{,}434.944}\ \text{GB}, \\ &\text{half kernel peak} \approx \mathbf{3{,}217.493}\ \text{GB}.\end{aligned}$$

E.2.4 Reconstructing the Decision Boundary (`BoundarySet-CCS`)

`BoundarySet-CCS` (Yang et al., 2024) selects samples *near the model's decision boundary* and then enforces *coverage* across distance bands. Distance-to-boundary is approximated per sample by the minimum number of PGD steps required to flip its prediction; `CCS` (coverage-centric sampling) then allocates the coreset budget across bands to preserve distribution coverage.

Execution. One-time selection with a proxy, then train the large model on the coreset for all T epochs:

i) *Train proxy:* train a proxy network on all N samples for T_{proxy} epochs (per-example forward cost f, parameters p).
ii) *Distance-to-boundary (PGD):* for each sample, run projected gradient steps until misclassification (cap at $K_{\max}$ steps). If the stopping step is k, define $d(x) = k$. Each PGD step requires one forward & one backward; we use $3f$ per step in our convention. Let $\bar{K} \leq K_{\max}$ be the average steps per sample.
iii) *CCS selection:* partition samples by $d(x) \in \{0, \ldots, K_{\max}\}$ and allocate the size-k budget across bands (linear-time bucketting and sampling).
iv) *Train large on coreset:* train the large model on the selected k points for *all* T epochs.

End-to-end compute (selection + coreset training).

$$\boxed{\text{Compute}_{\texttt{BoundarySet-CCS}} = \underbrace{3N\,T_{\text{proxy}}\,f}_{\text{train proxy}} + \underbrace{3N\,\bar{K}\,f}_{\text{PGD distance-to-boundary sweeps}} + \underbrace{3k\,T\,f_{\text{large}}}_{\text{train large on coreset}}}$$

Selection-stage storage overhead. Storage is mainly through the scalar distance per sample during selection:

$$\boxed{\text{StorageOverhead}_{\texttt{BoundarySet-CCS}} = \mathcal{O}(N) \;\; \text{(per-sample distance)}}$$

Example scenario values (ImageNet-1k; T_{proxy}=90, $K_{\max}$=50 so $\bar{K}\approx$50, T=90).

$$\text{Compute}_{\texttt{BoundarySet-CCS}}\ (\text{PFLOPs only}) \approx \underbrace{622.663}_{3NT_{\text{proxy}}f} + \underbrace{345.924}_{3N\bar{K}f} + \underbrace{280.061}_{3kT\,f_{\text{large}}} = \mathbf{1{,}248.648}\ \text{PFLOPs},$$

$\text{StorageOverhead}_{\texttt{BoundarySet-CCS}}$ (float32) $\approx N \times 4 = \mathbf{0.005}$ GB.

E.3 Training Property-based Methods

E.3.1 Samples with Low Loss Curvature (SloCurv)

SloCurv (Garg & Roy, 2023) scores each training sample by an *input-loss curvature* proxy computed at the end of (proxy) training. For a sample $\vec{z}_m$, with model parameters θ^T and random Rademacher directions v_r scaled by h, the score is

$$\text{Curv}(\vec{z}_m; \theta^T) \;=\; \frac{1}{R}\sum_{r=1}^{R} \left\| \nabla_{\vec{z}} \left[\ell\big(\theta^T, \vec{z}_m + hv_r\big) - \ell\big(\theta^T, \vec{z}_m\big) \right] \right\|_2^2 .$$

Samples with the lowest curvature are retained to form a size-k coreset.

Execution. One-time selection prior to training the large model; *a proxy model is used for scoring*:

i) *Train proxy:* train a proxy encoder with per-example forward FLOPs f and parameters p for T_{proxy} epochs on all N points.
ii) *Curvature scoring:* at the end of proxy training, for each sample compute $\text{Curv}(\vec{z}_m; \theta^T)$ using R Hutchinson repeats. This requires (R+1) gradient evaluations per sample (one at $\vec{z}_m$ and one for each $\vec{z}_m$+hv_r), each costing $\approx$ (1 fwd + 1 bwd) $\approx 3f$ in our convention.
iii) *Train on coreset:* select the k lowest-curvature samples and train the large model on this coreset for T_{late}=T epochs.

End-to-end compute (selection + coreset training).

$$\boxed{\text{Compute}_{\texttt{SloCurv}} = \underbrace{3N\,T_{\text{proxy}}\,f}_{\text{train proxy}} + \underbrace{3N\,(R{+}1)\,f}_{\text{curvature scoring at end of proxy training}} + \underbrace{3k\,T_{\text{late}}\,f_{\text{large}}}_{\text{train large on coreset}}}$$

Selection-stage storage overhead. Storage overhead is from keeping a track of the running curvature values and the directions probed.

$$\boxed{\text{StorageOverhead}_{\texttt{SloCurv}} = \mathcal{O}(N) \;+\; \mathcal{O}(Rd) \;\; (\text{running stats} + R \text{ probe dirs})}$$

Example scenario values (ImageNet-1k; T_{proxy}=90, T_{late}=90, R=10).

$$\text{Compute}_{\texttt{SloCurv}}\ (\text{PFLOPs only}) \approx \underbrace{622.663}_{3NT_{\text{proxy}}f} + \underbrace{76.103}_{3N(R+1)f} + \underbrace{280.061}_{3kT_{\text{late}}f_{\text{large}}} = \mathbf{978.827}\ \text{PFLOPs},$$

$$\text{StorageOverhead}_{\texttt{SloCurv}}\ (\text{float32}) \approx N \times 4 + Rd \times 4 = 11{,}094{,}540\ \text{B} = \mathbf{0.011}\ \text{GB}.$$

E.3.2 Temporal Dual-Depth Scoring (TDDS)

TDDS (Zhang et al., 2024) builds a coreset by combining two temporal depths of signal from training with a *proxy* model. Depth 1 computes, for each epoch, the projection of each sample's *per-sample gradient* onto the epoch's accumulated gradient direction. Depth 2 then aggregates these per-epoch contributions over a sliding window of length J and emphasizes their *temporal variability* (e.g., windowed variance). We maintain windowed statistics in a streaming manner (constant-time updates), so full trajectories need not be stored.

Execution. One-time selection with a proxy; the large model then trains on the coreset for the full T epochs:

i) *Train proxy:* train a proxy for T_{proxy} epochs on all N samples (per-example forward FLOPs f, parameters p); accumulate the epoch gradient direction.
ii) *Per-sample gradients:* after each proxy epoch, run a scoring sweep to compute per-sample gradients and their projections onto the epoch direction (costing one forward+backward per sample); update the J-length windowed statistics and TDDS score (streaming).
iii) *Select & train large:* rank by TDDS and keep the top-k; train the large model on these k samples for *all* T epochs.

End-to-end compute (selection + coreset training).

$$\boxed{\text{Compute}_{\texttt{TDDS}} = \underbrace{3N\,T_{\text{proxy}}\,f}_{\text{train proxy}} + \underbrace{3N\,T_{\text{proxy}}\,f}_{\text{per-sample gradient sweeps for TDDS}} + \underbrace{3k\,T\,f_{\text{large}}}_{\text{train large on coreset}}}$$

Selection-stage storage overhead. Streaming TDDS requires a J-length buffer of scalar contributions per example (and a temporary epoch-direction vector):

$$\boxed{\text{StorageOverhead}_{\texttt{TDDS}} = \ \mathcal{O}(NJ)\ \ \text{(windowed logs)}}$$

Example scenario values (ImageNet-1k; T=90, T_{proxy}=90, J=10).

$$\text{Compute}_{\texttt{TDDS}}\ (\text{PFLOPs only}) \approx \underbrace{622.663}_{3NT_{\text{proxy}}f} + \underbrace{622.663}_{\text{per-sample gradient sweeps}} + \underbrace{280.061}_{3kT\,f_{\text{large}}} = \mathbf{1{,}525.387}\ \text{PFLOPs},$$

$$\text{StorageOverhead}_{\texttt{TDDS}}\ (\text{float32}) \approx NJ \times 4 = 50{,}734{,}200\ \text{B} = \mathbf{0.051}\ \text{GB}.$$

E.3.3 Using Prediction Uncertainty with a Proxy (Dyn-Unc, DUAL)

Dyn-Unc (He et al., 2024) measures prediction uncertainty via a sliding window of length J over per-example target-class probabilities and averages the windowed uncertainty across proxy training.

DUAL (Cho et al., 2025) combines *uncertainty* with *difficulty* (window-mean prediction) and computes scores from an *early* stage of proxy training.

Execution. One-time selection with a proxy; the large model then trains on the coreset for the full T epochs:

i) *Train proxy:* train a proxy with per-example forward FLOPs f and parameters p for T_{proxy} epochs; maintain sliding-window statistics (length J) via $O(1)$ updates per visit.
ii) *Score & select:*

- `Dyn-Unc`: use windowed uncertainty (variance over the last J predictions), averaged over all proxy epochs T_{proxy}.
- `DUAL`: use the product of windowed uncertainty and difficulty (window mean), averaged over the *early* proxy epochs $T_{\text{proxy,early}} \leq T_{\text{proxy}}$.
- *Beta sampling* (`DUAL`): apply pruning-ratio–adaptive sampling based on a Beta distribution to stabilize extreme pruning. This adds negligible compute and storage.

iii) *Train on coreset (large model):* train for *all* T epochs on the top-k points.

End-to-end compute (selection + coreset training).

$$\boxed{\begin{aligned}\text{Compute}_{\texttt{Dyn-Unc}} &= \underbrace{3N\,T_{\text{proxy}}\,f}_{\text{train proxy + logging}} + \underbrace{3k\,T\,f_{\text{large}}}_{\text{train large on coreset}}, \\ \text{Compute}_{\texttt{DUAL}} &= \underbrace{3N\,T_{\text{proxy,early}}\,f}_{\text{early proxy scoring}} + \underbrace{3k\,T\,f_{\text{large}}}_{\text{train large on coreset}}.\end{aligned}}$$

Selection-stage storage overhead. Only require a scalar window of values per example.

$$\boxed{\begin{aligned}\text{StorageOverhead}_{\texttt{Dyn-Unc}} &= \mathcal{O}(NJ), \\ \text{StorageOverhead}_{\texttt{DUAL}} &= \mathcal{O}(NJ).\end{aligned}}$$

Example scenario values (ImageNet-1k; T=90, T_{proxy}=90, $T_{\text{proxy,early}}$=50, J=10).

$$\text{Compute}_{\texttt{Dyn-Unc}}\ (\text{PFLOPs only}) \approx \underbrace{622.663}_{3NT_{\text{proxy}}f} + \underbrace{280.061}_{3kT\,f_{\text{large}}} = \mathbf{902.724}\ \text{PFLOPs},$$

$$\text{Compute}_{\texttt{DUAL}}(\text{PFLOPs only}) \approx \underbrace{345.924}_{3NT_{\text{proxy,early}}f} + \underbrace{280.061}_{3kT\,f_{\text{large}}} = \mathbf{625.985}\ \text{PFLOPs},$$

$$\text{StorageOverhead (float32)} \approx NJ \times 4 = \mathbf{0.051}\ \text{GB for each.}$$

E.4 Our Method - Correlation of Loss Differences (`CLD`)

`CLD` builds a coreset by leveraging only *loss values* over training: it records the per-epoch losses of all training points and a small held-out query set, then ranks training examples using the correlation of loss *differences* across epochs between train and query. No gradients or Hessians are required.

Execution. One-time selection with a proxy, followed by large-model training:

i) *Train proxy:* train a proxy model for T_{proxy} epochs on all N samples (per-example forward cost f, parameters p).

ii) *Collect losses:* during proxy training, record per-epoch losses for all N training samples (no extra compute beyond the training pass), and run a forward pass on all Q query samples each epoch to record their losses (Qf FLOPs per epoch).

iii) *Score & select:* compute `CLD` scores (correlations of loss differences over epochs) and select a size-k coreset. The arithmetic for correlations/ranking is linear-time in the number of stored losses and is negligible compared to FLOPs above.

iv) *Train on coreset:* train the large model on the selected k points for T epochs.

End-to-end compute (selection + coreset training).

$$\boxed{\text{Compute}_{\texttt{CLD}} = \underbrace{3N\,T_{\text{proxy}}\,f}_{\text{train proxy}} + \underbrace{Q\,T_{\text{proxy}}\,f}_{\text{query loss collection}} + \underbrace{3k\,T\,f_{\text{large}}}_{\text{train large on coreset}} \quad (\text{FLOPs})}$$

Selection-stage storage overhead. We store loss scalars for all N training and Q query samples across T_{proxy} epochs:

$$\boxed{\text{StorageOverhead}_{\texttt{CLD}} = \mathcal{O}\big((N{+}Q)T_{\text{proxy}}\big) \;\; \text{(loss logs)}}$$

Example scenario values (ImageNet-1k; T_{proxy}=90, T=90).

$$\text{Compute}_{\texttt{CLD}} \text{ (PFLOPs only)} \approx \underbrace{622.663}_{3NT_{\text{proxy}}f} + \underbrace{2.097}_{QT_{\text{proxy}}f} + \underbrace{280.061}_{3kT_{\text{late}}f_{\text{large}}} = \mathbf{904.821} \text{ PFLOPs},$$

$$\text{StorageOverhead}_{\texttt{CLD}} \text{ (float32)} \approx (N{+}Q)T_{\text{proxy}} \times 4 = 461{,}220{,}120 \text{ B} = \mathbf{0.461} \text{ GB}.$$

F Comparison of CLD with Influence

The impact measured by CLD closely aligns with the "*influence*" of individual training samples on a model's predictions that are measured by *Training Data Attribution* (TDA) methods. TDA methods have been widely employed for tasks such as debugging datasets, interpreting models, and optimizing training efficiency Koh & Liang (2017); Yeh et al. (2018); Feldman & Zhang (2020).

The earliest TDA methods utilized *Leave-One-Out* (LOO) training, which involves retraining the model after removing specific data points and observing the changes in performance. While straightforward, LOO retraining is computationally prohibitive for modern deep learning models due to the need for multiple retraining cycles Koh & Liang (2017). Recent TDA metrics, such as FZ-Influence (Infl) Feldman & Zhang (2020) and Datamodels Ilyas et al. (2022), have gained popularity owing to precomputed scores for widely-used datasets in computer vision. These methods, however, face scalability challenges.

A prominent alternative that arose was *Influence Functions*, which estimated the effect of downweighting individual samples using first-order (gradient) and second-order (Hessian) computations Koh & Liang (2017); Basu et al. (2021) performed at the end of training. Methods like RandSelect Wojnowicz et al. (2016) and Arnoldi iterations Schioppa et al. (2022) improved computational efficiency by approximating the Hessian. Similarly, TRAK Park et al. (2023) combined random projections, gradient-based methods, and ensembling to estimate the influence of training samples. However, these approaches often rely on strong assumptions, such as convergence to a unique optimal solution, which limits their applicability to neural networks. Additionally, Hessian computations introduce significant computational overhead. To address these challenges, *unrolling-based* methods that observe the learning process across training iterations have been proposed. These techniques approximate the impact of samples by differentiating through the optimization trajectory Hara et al. (2019). Among these, TracIn Pruthi et al. (2020) is a highly efficient method that estimates influence using gradients tracked throughout training. Its practical implementation, TracInCP, uses intermediate checkpoints to alleviate computational burdens. While effective, unrolling methods require storing intermediate training states, leading to high storage and computational costs.

In contrast, CLD solely relies on loss trajectories rather than first- or second-order quantities (e.g., gradients and Hessians).

In order to measure the "influence" of a training sample $\vec{z}_m$ on an individual unseen (or query) sample $\vec{z}_q$, we modified Definition 1 slightly to be

$$\texttt{CLD}_{\texttt{infl}}(\vec{z}_m, \vec{z}_q) \coloneqq \rho\left(\vec{\Delta}_m, \vec{\Delta}_q\right) \tag{64}$$

We will now compare the impact measured by this metric ($\texttt{CLD}_{\texttt{infl}}$) to the influence measured by TDA metrics, by utilizing the *linear datamodeling score* (LDS) introduced by Park et al. (2023). LDS measures the correlation between group-level attribution scores ($\texttt{CLD}_{\texttt{infl}}$ or influence) and their observed impact on model predictions when subsets of training data are used.

LDS definition For a query data point z_q, random subsets $\{\mathcal{S}_j\}_{j=1}^{C}$ are sampled from the training dataset, where each subset $\mathcal{S}_j$ contains $\lceil \alpha N \rceil$ points, with $\alpha \in (0, 1)$ as the sampling ratio. Each subset $\mathcal{S}_j$ is used to retrain the model R times with different initializations $\{\xi_r\}_{r=1}^{R}$ and training parameters λ, resulting in

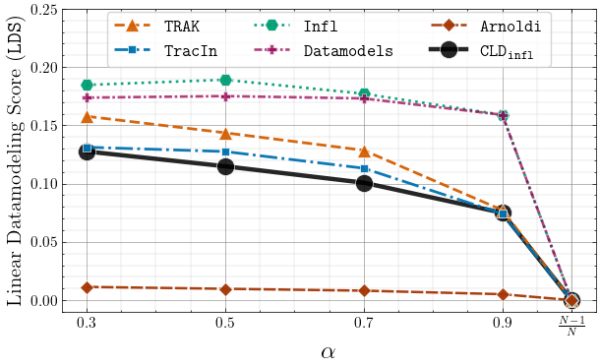

(a) Linear datamodeling scores (LDS) of existing TDA metrics compared to $\texttt{CLD}_{\texttt{infl}}$. The scores were evaluated on CIFAR-10, ResNet-9 with 200 (randomly selected) query samples evaluated over 100 subsets.

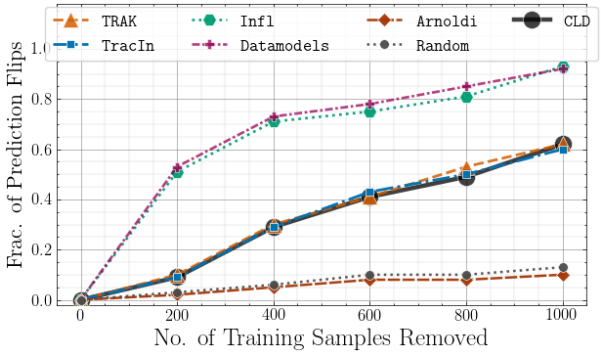

(b) Prediction brittleness of CLD and TDA metrics on CIFAR-10 with ResNet-9. The top-k influential training samples were removed, and the average prediction flips for 200 query samples over 5 seeds are shown.

Figure 8: Comparison of CLD to TDA metrics. (Best viewed in color.)

the model $\theta^T_{S_j,\xi_r}$. This trained model is then used to compute a measurable quantity $f(\vec{z}_q, \theta^T_{S_j,\xi_r})$. A *group attribution score*, $g_\tau(\vec{z}_q, \mathcal{S}_j, \mathcal{S})$, is calculated as $g_\tau(\vec{z}_q, \mathcal{S}_j, \mathcal{S}) \coloneqq \sum_{\vec{z}\in\mathcal{S}_j} \tau(\vec{z}_q, \vec{z}, \mathcal{S})$, where $\tau(\vec{z}_q, \vec{z}, \mathcal{S})$ is the attribution score for a training point $\vec{z}$ with respect to $\vec{z}_q$. The LDS is then obtained using Spearman's rank Spearman (1904) correlation (ρ_s):

$$\texttt{LDS}(\vec{z}_q, \alpha) \coloneqq \rho_s\left(\left\{\frac{1}{R}\sum_{r=1}^{R} f\left(\vec{z}_q, \theta^T_{S_j,\xi_r}\right)\right\}_{j=1}^{C}, \{g_\tau\left(\vec{z}_q, \mathcal{S}_j, \mathcal{S}\right)\}_{j=1}^{C}\right) \tag{65}$$

Experimental Setup: We compared the LDS scores of $\texttt{CLD}_{\texttt{infl}}$ against those of TRAK, Arnoldi, TracIn, Infl, and Datamodels. Precomputed scores for Infl and Datamodels were used for the CIFAR-10 dataset Krizhevsky et al. (2009) with ResNet-9 He et al. (2016), while 10 models were trained for TRAK, Arnoldi, TracIn, and $\texttt{CLD}_{\texttt{infl}}$. The evaluation employed $C = 100$ random subsets, sampling ratios α ranging from 0.3 to $\frac{N-1}{N}$, a query set of 200 samples, and $R = 10$ seeds. The measurable quantity was the accuracy of query samples.

Results and Observations: The results presented in Figure 8a reveal that while the impact captured by $\texttt{CLD}_{\texttt{infl}}$ is distinct from the influence measured by traditional TDA metrics, it aligns closely with methods such as TracIn and TRAK in terms of behavior while being resource-efficient. Notably, the performance gap between these computationally intensive methods and $\texttt{CLD}_{\texttt{infl}}$ narrows as α increases. The drop in LDS scores at $\alpha = \frac{N-1}{N}$ is due to the stochastic nature of model retraining[1].

Takeaways: Although $\texttt{CLD}_{\texttt{infl}}$ (and in essence CLD) fundamentally differs from influence-based TDA metrics, it mirrors their trends at higher sampling ratios while maintaining superior computational efficiency, solidifying its utility as a practical tool for analyzing training dynamics.

F.1 Importance of the Top-k Samples

We demonstrate that the samples identified by CLD are indeed pivotal for generalization, addressing the question: *"Are the training samples with the top-k scores truly the most critical for forming a coreset?"* This is evaluated using the *prediction brittleness* metric. This is also mentioned briefly in Section 8.

Experimental Setup: To quantify the influence of top-k samples, we systematically removed the most impactful data points identified by their CLD scores, from the training set and retrained the model. The metric of interest was the fraction of prediction flips observed in a held-out query set after retraining. If these samples are truly critical for generalization, their removal should cause substantial prediction changes. This experiment also included a comparative analysis with the top-k influential samples identified by TDA

[1]This observation is consistent with the findings of previous research Karthikeyan & Søgaard (2021); Bae et al. (2024).

scores, discussed in this section. Experiments were performed on the CIFAR-10 dataset using a ResNet-9 architecture, with a randomly selected query set of 200 samples. For each configuration, once the top-k samples were excluded, the model was retrained 5 times to account for randomness, and the average fraction of prediction flips was recorded.

Results and Observations: The results, summarized in Figure 8b, illustrate that the top-k samples identified by `CLD` have a comparable influence on prediction outcomes to those identified by TDA-based metrics such as `TracIn` and `TRAK`. Notably, removing the top-800 samples of CIFAR-10, which constitutes just 1.6% of the dataset, results in prediction flips for over half of the query set. This highlights the significant role of the samples identified by `CLD` in supporting model generalization. While metrics like `Datamodels` and `Infl` exhibit greater impact, they are computationally prohibitive, rendering them unsuitable for large-scale coreset generation.

Takeaways: `CLD` emerges as an effective and computationally efficient approach for identifying training samples critical to generalization, making it a practical tool for coreset selection in large-scale machine learning pipelines.